

# UNIVERSITA' DEGLI STUDI DI NAPOLI "FEDERICO II"



## FACOLTA' DI INGEGNERIA

Dipartimento di Ingegneria Chimica, dei Materiali e della Produzione  
Industriale D.I.C.MA.P.I.

Dottorato di Ricerca in Ingegneria dei Materiali e delle Strutture

XXVIII ciclo

## **“Guiding stem cell self-organization and differentiation through material nanopatterning”**

### ***Coordinatore***

*Prof. G. Mensitieri*

### ***Tutor***

*Prof. P.A. Netti*

### ***Candidata***

*Lucia Formisano*

# Table of Contents

<b>1 Introduction</b>	5
<b>2 Nanoengineered surfaces for self-organized aligned cell sheet formation</b>	14
2.1 Introduction	14
2.2 Results and discussion	17
2.2.1 Effect of surface topography and adhesivity on hMSC behaviour	17
2.2.2 Effect of substrate stiffness on hMSCs self-organization	22
2.2.3 Scanning Electron Microscopy (SEM) analysis	25
2.2.4 Molecular profile analysis of hMSC constituting cell sheets	27
2.3 Conclusions	34
2.4 References	36
<b>3 Engineered material surfaces to control tissueogenesis</b>	39
3.1 Introduction	39
3.2 Results and discussion	40
3.2.1 Single and collective cell dynamics	40
3.2.2 Effect of surface adhesivity on hMSC behaviour	43
3.2.3 Effect of contractility on hMSC self organization and tissue formation	46
3.2.4 Characterization of Fibrillar Collagen by Picrosirius Red (PSR)	47
3.2.5 Transmission electron microscopy (TEM) examination	48
3.2.6 Second Harmonic Generation (SHG) microscopy for analysis of collagen fibrillar structure	51
3.2.7 Molecular profile analysis by RT-PCR	52
3.3 Conclusions	54
3.4 References	59
<b>4 Materials and methods</b>	61
4.1 Preparation of nanopatterned substrates	61
4.2 Functionalization of patterned surfaces	61
4.3 Cell culture	62
4.4 Drug treatment	63
4.5 Time lapse video microscopy	64
4.6 Confocal and multiphoton microscopy	64
4.7 Image analysis	65
4.8 Characterization organization of the collagen fibers	66
4.9 Second harmonic generation	66
4.10 Transmission electron microscopy (TEM)	67
4.11 Scanning electron microscopy (SEM)	68
4.12 Nano-indentation test	69
4.13 Real Time-PCR	69

## Abstract

Biophysical stimuli in the local microenvironment proved to be effective in influencing various aspects of cell behavior such as adhesion, spreading, migration and differentiation [1]. In particular, many studies focused on biomaterials with nanometric scale surface topography able to dictate specific cell shapes, which in turn control cell fate and functions through mechanotransduction pathways [2]. While the role of biophysical signals and more specifically of topographic signals on single cell behavior is well established, there are comparatively less studies on their role on the collective cell behavior. In particular it is not clear how biophysical signals may affect cells self-organization into a three-dimensional tissue.

Here, we used nanopatterned substrates able to control adhesion and contractility processes to generate ordered tissues in vitro. In particular we show that by changing the combination of the initial conditions for cell adhesion we obtained different cell behaviours in terms of self-organization and subsequent tissue development. Bone-marrow-derived hMSCs were cultured on polydimethylsiloxane (PDMS) substrates containing parallel and straight channels having ridge to groove width ratio of 1:1, previously treated with the oxygen plasma, that increases the hydrophilicity, improving cell adhesion. Pattern features used, were 350 nm width and depth of 100 nm. Focal adhesions, cytoskeleton and matrix production were visualized with confocal, scanning electron and transmission electron microscopy. Expression of relevant genes was assessed by RT-PCR analysis. In this culturing setup, hMSCs proliferated and organized into dense cells sheets displaying a multi-level order. Molecular analysis suggests that these conditions create a microenvironment that allows the maintenance of stemness and the enhance of the expression of the pluripotency genes into hMSC.

By modifying the initial conditions, dramatically changes the cellular behavior were observed. In fact, by increasing the size of the topographic patterns (channels of 700

nm width and 250 nm depth), without surface chemical treatments, the hMSC were stimulated to arrange themselves into self-organized structures that shared similarities with the tendon tissue, in terms of macroscopic morphology, internal cellular organization and molecular profile. These data suggest that the pattern provides an initial guidance for FAs and subsequent cell alignment. Aligned cells exert a polarized contractility that leads to the formation of ordered structures.

In conclusion, our results demonstrate that the chemical-physical characteristics of the substrate, were able to strongly affect cell behavior in terms of cell fate and in vitro generated tissue functions.

In conclusion, nanoengineered material surfaces can be in principle employed to set off the hMSC program toward tissue genesis in a deterministic manner by using the correct combination of initial biophysical signals.

## References

1. Ventre et al. *J R Soc Interface*, 9, 2017-2032, 2012
2. McNamara et al. *J Tissue Eng*, 120623, 2012

## 1. Introduction

In the last years, scientific research in the field of tissue engineering has turned its attention to the contribution of signals which are naturally provided by the tissue microenvironment on the commitment of stem cells.

Classically, the control on the stem cells fate, both in vivo and in vitro, was mainly attributed to genetic and molecular mediators such as growth factors, hormones and transcription factors. However, in the absence of these factors a wide range of other environmental factors contribute to the overall control of the activity of stem cells, for example the extracellular matrix (ECM) structure and its mechanical properties. Several works demonstrated the relevance of this concept in the case of stem cells that are very sensitive to microenvironment signals [1, 2]. In fact, signals presented to stem cells in their niche, ultimately dictate fate and functions i.e. whether they have to remain quiescent, proliferate or differentiate [3].

The cells can establish different mechanisms of interaction with the ECM in vivo as well as with a scaffold in vitro to activate a particular cellular function (such as adhesion, migration, etc.). This occurs owing to the interaction between molecules such as ligands and receptors that activate a signaling pathway that changes the cell itself and the environment that surrounds it [4].

The Focal Adhesion (FA) is a common type of adhesive contact that cells make with the ECM and are composed of large and dynamic protein complexes that mediate the link between the cell cytoskeleton and the extracellular matrix. This connection generally involves a class of integral membrane glycoproteins called integrins, heterodimers containing one  $\alpha$ - and one  $\beta$ - subunit.

Into the cell, the extracellular domain of integrin binds the actin cytoskeleton through membrane proteins such as mechanical sensors (talin and vinculin), signaling proteins (focal adhesion kinase- FAK, ad paxillin ) and links to the cytoskeleton (actinin and zyxin).

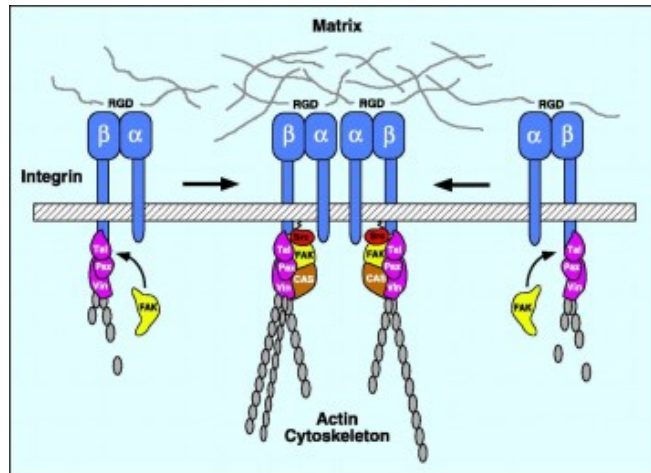


**Figure 1.** Illustration of the interaction between integrins and the actin cytoskeleton.

Nascent adhesion may either disassemble or mature into larger molecular structures called focal complexes that are 0,5  $\mu\text{m}$  wide and up to 10  $\mu\text{m}$  long. This requires clustering of additional integrin dimers, which increases the dimension of the adhesion assembly and allows the recruitment of more cytoplasmic adhesion proteins that stabilize the construct.

In addition to their adhesive functions, integrins mediate bidirectional signalling between the cell and the ECM, activating both direct mechanotransductive signaling and indirect molecular cascades that regulate transcription factor activity, gene and protein expression, and ultimately growth and differentiation [5]

Therefore, the transduction of external mechanical signals (including cell stretch, compression and interaction with topography) within the cell, i.e. mechanotransduction, requires an appropriate set of interactions between the cell and its microenvironment resulting in adaptive gene- and protein-level change.

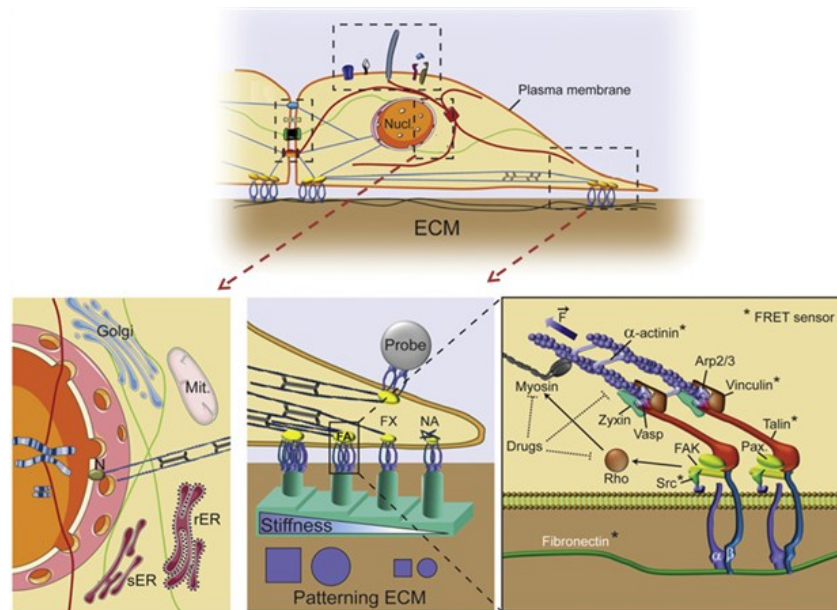


**Figure 2.** Representation of the possible effects of cytoskeleton-generated forces on intracellular events. (Adapted from Eyckmans J, Boudou T, Yu X, Chen CS. A hitchhiker's guide to mechanobiology. *Dev Cell*. 21, 35-47, 2011)

In this context, cell adhesion acquires a central role in the perception of topography, stiffness and ligand positioning of the ECM, representing the initiating event in many complex biological processes, such as morphogenesis, organogenesis, tissue repair and tumor progression [2].

Tissue morphogenesis results from the formation of adhesive contacts between cells and between cells and matrix, a process that requires a cooperation between adhesive systems and the actin cytoskeleton [6].

Such adhesion mechanisms are highly regulated during tissue morphogenesis and intimately related to the processes of cell motility and cell migration.

In vivo, the cells are free to migrate through the ECM and may reshape the matrix by means of mechanical forces or chemical modifications, thus generating a variety of forms each suitable to the functional requirements of a different tissue.

In vitro, cell-cell and cell-material interactions can be manipulated in order to mimic the native environment and eventually leading to the formation of tissues or ordered

supracellular structures.

Several studies have shown that the formation of the FA and the effects on the cell cytoskeleton define the necessary force to sculpt the tissue [7, 8, 9], but how to modulate the FA spatial distribution and the force levels to generate a desired tissue is still unclear.

The behavior of stem cells *in vivo* is crucially influenced by their interactions with the various biochemical and biophysical niche components, which underlines the importance of the microenvironment in regulating stem cell fate. This is well-illustrated by the case of embryoid bodies (EBs), aggregates of pluripotent stem cells cultured in suspension which have been used to model early development and patterning of the embryo [10].

The recently introduced stem cell-derived organoids have demonstrated that, aside from modeling early embryogenesis, stem cells can be used to mimic aspects of rodent and human organogenesis. Organoids are derived from pluripotent stem cells or isolated organ progenitors that differentiate to form an organlike tissue exhibiting multiple cell type that self-organize to form a structure not unlike the organ *in vitro* [11].

Although stem cell-derived organoids recapitulate a much wider range of cellular and developmental phenomena compared with traditional 3D culture, differences from the native organs still exist, suggesting that microenvironmental components are either lacking or presented incorrectly in space and time. A major difference between organogenesis *in vivo* and *in vitro* lies in the mode by which signals are presented to cells. Whereas the native microenvironment delivers cues with a high degree of spatiotemporal control, traditional 3D culture floods cells with biochemical and biophysical signals that are uniform in space and static in time [12].

Advances in biomaterials technologies, that mimic the spatiotemporal complexity of the *in vivo* microenvironment, can potentially be used to reconcile these differences

and to modulate tissue formation with a greater degree of control than previously achieved.

While organoid development requires the conditioning of pluripotent cells, mesenchymal stem cells (MSCs) remain the most used cells in tissue engineering (TE) applications. These cells generated a great interest due to their ability to replicate in culture while maintaining the ability to differentiate into specific cell lines such as bone cells (osteoblasts), cartilage cells (chondrocytes), tendon cells (tenocytes) and fat cells (adipocytes) [13]. Yet, their use in the generation of functional tissues in vitro, similar to what observed in organoids, has seen alternate fortunes.

MSC fate is very sensitive to exogenous signals and biophysical signals proved to be effective in altering cell differentiation.

Many studies focused the attention on biomaterials with nanometric scale surface topography able to affect cell adhesion and morphology by physical confinement or contact guidance [14, 15, 16]. Cells sense and respond to such stimuli and interpret changes of the physical properties of the substrates as changes of adhesion-ligand presentation.

The molecular mechanisms underlying the biophysical control of cell fate are not thoroughly clear but there is growing evidence that FA formation and maturation, contractility and cell shape play an important role in the process of differentiation. For example, Yim et al. [17] demonstrated that nanograted substrata were able to induce transdifferentiation of hMSCs in neurons.

While these studies were instrumental in improving our understanding of cell signals interactions, the use of biophysical signals to specifically control morphogenesis is still far to come. For instance, three-dimensional culture systems have been developed to direct the formation of spheroids, groups of rounded cells, because it has been seen that this morphology is critical in the stem cells differentiation in chondrocyte phenotype [18]. Evidently, the morphology and, in particular, the shape taken from

the nucleus in cells cultured in such systems, is reflected on the expression of typical gene markers of cartilage tissue.

Zhu et al report that, primary porcine tenocytes cultured on microgroove silicone membrane maintain the expression of tenomodulin (marker tenocyte) and collagen I (functional molecule) while tenocytes cultured on the flat surface of the plate have lost or significantly reduced the expression of tenomodulin or collagen I [19].

A few examples demonstrate that micro- and nanopatterning can effectively impact on the organization and functions of tissues grown in vitro. ECM-rich tissues with an ordered structure were obtained by Guillemette et al., who demonstrated that elastomeric microgratings with a 4  $\mu\text{m}$  periodicity induced corneal fibroblast to form a collagen rich multilayer, whose microarchitecture was analogous to the lamellar structure of native cornea [20]

These data suggest that patterning adhesion signals not only direct lineage specification, but might in principle direct cell self-organization and tissueogenesis in vitro.

Today there are several techniques for the manufacture of nano-structured materials, such as the photolithography and the electron beam lithography. These techniques have been highly developed for the micro-electronics industry but have been adapted also to biological studies with various degrees of success. For example soft lithography solves many of the problem that required the application of microfabrication to biological problems.

With these techniques it is possible to create topographical features that the cells are able to sense. The typical nanogrooves products can be described as channels that cells use as a guide in the early phases of the interaction with the scaffold. As a result of this interaction occurs a reorganization of integrins expressed in membrane which results in the change, in terms of size and number, of focal adhesion and complex.

Therefore, topographical pattern acts as a guide on cell adhesion and migration because the topographic features, through a confining effect, induces alignment and spatial distribution of FAs. Ordered arrays of FAs cause the cytoskeleton to assemble in elongated and oriented along the pattern.

In this way, knowing the architecture of one tissue, it is possible to design the scaffold with the most appropriate topographic features in order to direct the cells to assume exactly the same organization that they present in vivo.

Not surprisingly, topographic patterns have also a great impact on the collective behaviour of cell population. In more details, nanogrooves have the ability of polarizing confluent cell layers, i.e. cells display a common, spindle-like orientation, thus inducing an order on the matrix the cells produce [20]. These results might be relevant for the production of ordered tissue in vitro, as well as for an improved integration of prostheses and scaffold in vivo settings.

In the present work, the influence of biophysical and more specifically of topographical signals are examined as a means to modulate the processes of organization and cell differentiation by generating three-dimensional tissues in vitro, with particular focus on mesenchymal stem cells.

We showed that by modulating the combination of initial conditions in terms of cell adhesion on synthetic substrates it is possible alter the tissue organization and microarchitecture. Furthermore, the characteristics of the new matrix produced by the cells are able to strongly affect cell behavior in terms of cell fate and in vitro generated tissue functions.

To address the mechanistic basis underlying the topographical effects on stem cells, we have devised and implemented microstructural and morphological characterization essays and data from molecular analysis is also outlined in relation to topography-mediated fate determination.

## References

1. Dalby MJ, Gadegaard N, Oreffo RO. Harnessing nanotopography and integrin-matrix interactions to influence stem cell fate. *Nat Mater.* 2014; 13:558-69.
2. Jansen KA, Donato DM, Balcioglu HE. A guide to mechanobiology: Where biology and physics meet. *Biochim Biophys Acta.* 2015; 1853:3043-52.
3. Khetan S, Guvendiren M, Legant WR, Cohen DM, Chen CS, Burdick JA. Degradation-mediated cellular traction directs stem cell fate in covalently crosslinked three-dimensional hydrogels. *Nat Mater.* 2013; 12:458-65.
4. Geiger B, Yamada KM. Molecular architecture and function of matrix adhesions. *Cold Spring Harb Perspect Biol.* 2011; 3(5).
5. Ingber DE. Cellular mechanotransduction: putting all the pieces together again. *FASEB J.* 2006; 20:811-27.
6. Mammoto T, Mammoto A, Ingber DE. Mechanobiology and developmental control. *Annu Rev Cell Dev Biol.* 2013; 29:27-61.
7. McBeath R, Pirone DM, Nelson CM. Cell shape, cytoskeletal tension, and RhoA regulate stem cell lineage commitment. *Dev Cell.* 2004; 6:483-95.
8. Huebsch N, Arany PR, Mao AS, Shvartsman D, Ali OA, Bencherif SA. Harnessing traction-mediated manipulation of the cell/matrix interface to control stem-cell fate. *Nat Mater.* 2010; 9:518-26.
9. Dalby MJ, Gadegaard N, Tare R, Andar A, Riehle MO, Herzyk P, Wilkinson CD, Oreffo RO. The control of human mesenchymal cell differentiation using nanoscale symmetry and disorder. *Nat Mater.* 2007; 6:997-1003.
10. Itskovitz-Eldor J, Schuldiner M, Karsenti D, Eden A, Yanuka. Differentiation of human embryonic stem cells into embryoid bodies compromising the three embryonic germ layers. *Mol Med.* 2000:88-95.
11. Lancaster MA, Knoblich JA. Organogenesis in a dish: modeling development and disease using organoid technologies. *Science.* 2014;345:1247125.

12. Gjorevski N1, Ranga A, Lutolf MP. Bioengineering approaches to guide stem cell-based organogenesis. *Development*. 2014; 141:1794-804.
13. Meirelles LdS, Chagastelles PS, Nardi NB (2006) "Mesenchymal stem cells reside in virtually all post-natal organs and tissues". *J Cell Sci*, 119.
14. Zhu, B., Zhang, Q., Lu, Q., Xu, Y., Yin, J., Hu, J. & Wang, Z. (2004) "Nanotopographical guidance of C6 glioma cell alignment and oriented growth". *Biomaterials* 25.
15. Engler AJ, Sen S, Sweeney HL, Discher DE (2006) "Matrix elasticity direct stem cell lineage specification". *Cell*, 126.
16. Dalby MJ, Gadegaard N, Tare R, Andar A, Riehle MO, Herzyk P, W. The control of human mesenchymal cell differentiation using nanoscale symmetry and disorder. *Nat Mater*. 2007; 6:997-1003.
17. Yim, E. K., Pang, S. W., Leong, K. W. (2007) "Synthetic nanostructures inducing differentiation of human mesenchymal stem cells into neuronal lineage". *Exp. Cell Res*. 313.
18. Herlofsen S, K uchler A, Egil Melvik J, Brinchmann J (2011) "Chondrogenic Differentiation of Human Bone Marrow-Derived Mesenchymal Stem Cells in Self-Gelling Alginate Discs Reveals Novel Chondrogenic Signature Gene Clusters". *Tissue Eng Part A*. 2011; 17:1003-13.
19. Zhu J, Li J, Wang B, Zhang W, Zhou G, Cao Y, Liu W (2010) "The regulation of phenotype of cultured tenocytes by microgrooved surface structure". *Biomaterials*. 2010; 31:6952-6958.
20. Guillemette MD, Cui B, Roy E, Gauvin R, Giasson CJ, Esch MB, Carrier P, Deschambeault A, Dumoulin M, Toner M, Germain L, Veres T, Auger FA. Surface topography induces 3D self-orientation of cells and extracellular matrix resulting in improved tissue function. *Integr Biol (Camb)*. 2009, 1:196-204.

## **2. Nanoengineered surfaces for self-organized aligned cell sheet formation**

### **2.1 Introduction**

The biophysical and biochemical signals displayed by material surfaces are able to affect many aspects of cell behavior such as adhesion, spreading, migration, proliferation and differentiation. Thus, a better knowledge of how cells sense and respond to mechanical signals at molecular level is necessary to understand the process by which physical forces regulate tissues development.

In an *in vivo* context, cells are highly sensitive to the architecture of the surrounding microenvironment and in particular the mechanical interactions between cells and between cell and ECM affect cell responses. Similarly, *in vitro* context, material surfaces can be in principle engineered in terms of rigidity, surface roughness, ligand density and availability, topography and hydrophobicity in order to mimic the conditions of the natural environment to control and guide cell fate and functions. Many studies focused the attention on biomaterials with nanometric scale surface topography able to affect cell adhesion and morphology by physical confinement or contact guidance [1, 2, 3]. Cells sense and respond to such stimuli and interpret changes of the physical properties of the substrates as changes of adhesion-ligand presentation.

In this regard, Yim et al. [4] demonstrated the significance of nanotopography in directing differentiation of hMSCs showing that the combination of nanotopography and biochemical cues such as retinoic acid up-regulated neuronal marker expressions, but nanotopography showed a stronger effect compared to retinoic acid alone on unpatterned surface.

However the understanding of mechanisms involved in cell responses to these signals expressed on the material surfaces is complex and, while the effect of nanopatterning

has been widely investigated in the context of single cell behavior, the role exerted by topographic signals on the dynamic self-organization of cell is still unclear.

The processes of self-assembly and self-organization of undifferentiated cells is a key features that gives rise to differentiated and functional organoids in vitro. However, the role played by exogenous stimuli and, in particular by material cues in regulating those processes has not been characterized in details.

Recent studies showed that by combining self-organizing stem cells with the biomaterials and microtechnology approaches it is possible to increase the fidelity with which in vitro-derived organoids replicate their corresponding native organs, while also enabling additional control over the process [5].

Organogenesis and morphogenesis involve dynamic remodeling of the ECM. In addition to the physical connection of cells within tissues, ECM acts as 3D scaffold that resist to cell-traction forces and thereby regulate tissue development by altering physical force distributions modulating cell shape [6, 7, 8].

Many morphogenetic events, such as oriented cell division and migration, depend on the assembly of ECM. For example, fibronectin (FN) fibrillogenesis is necessary to maintain orientated cell division and cell polarity in embryogenesis [9]. This suggests that proper spatiotemporal expression and assembly of ECM structures play key role in the regulation of morphogenesis. Vogel et al. [10] demonstrated that cell traction forces exerted on ECM via bound integrins also induce physical unfolding of some ECM molecules, such as FN and collagen. These force-depend change in molecular conformation expose cryptic sites that promote ECM fibrillogenesis, which can feed back to activate intracellular signaling pathway that alter cell proliferation and ECM turnover. The control of ECM-driven cell migration is essential for directing cells to their appropriate destinations where they assemble into specialized tissues.

The stiffness of the matrix plays an equally important role. The rigidity of the ECM not only stabilizes various tissues and organs but also controls stem cell self-renewal and

lineage switching, which are crucial for organogenesis and regeneration. Engler and coworkers [11], in a study with stem cells, showed that variations in ECM mechanics direct mesenchymal stem cells (MSCs) along different cell lineages. For example, MSCs differentiate into a neuronal-like lineage when grown on soft ECM gels, but they differentiate into osteoblasts on stiff gels and into myoblast on ECMs with intermediate stiffness.

In a different application, Rowlands et al. evaluated the adhesion and spreading of Bone Marrow Stromal Cells (BMSCs) on various polyacrylamide gel substrates, with ranging from 0.7 to 80 kPa, previously coated with fibronectin [12]. They found that high stiffness of about 80 kPa promotes cell adhesion and spreading.

Here, we investigated how the combined effect of substrate stiffness, topography and surface adhesivity affects hMSCs behaviour in terms of supracellular self-organization and three-dimensional tissue formation.

Our hypothesis is that by combining the substrate properties, the development of the tissues can be modulated and the crosstalk between the signals presented by the materials and the signals produced by the cells could influence the stem cells behavior and fate.

The aim of the work reported in this chapter is to evaluate the effect of these signals on the cell self-organization, molecular profile and tissue production. In particular, we showed that by changing the combination of initial conditions for cell adhesion we obtained different cell behaviours in terms of cell self-organization and tissue development. In more details, we cultured hMSCs on polydimethylsiloxane (PDMS) substrates containing parallel and straight channels having ridge to groove width ratio of 1:1, without the employment of growth factors or exogenous scaffold matrices. The pattern features used were 700nm wide or 350nm wide and depth of 250 nm or 100 nm respectively. These pattern dimensions are well known for their ability to affect the cell alignment and polarization [13]. Once established the appropriate

topographic features, we modulated also the mechanical properties in terms of substrates stiffness. In particular, we obtained three different stiffness by modulating base and curing agent weight ratio during PDMS preparation. Moreover, we modulated the levels of cell adhesivity in terms surface hydrophilicity and protein adsorption by means of oxygen plasma treatment.

## 2.2 Results and discussion

### 2.2.1 Effect of surface topography and adhesivity on hMSC behaviour

Different initial conditions, in term of ligand density, availability and positioning, correlate with a different cell behaviour in a context of single cell, but the effects on the collective cell behaviour remain unknown. To investigate how hMSCs translate the changes of biochemical and biophysical properties of their environment into signals that regulate the tissue self-organization, quasi-confluent hMSCs populations were seeded on arrays of PDMS nanopatterned surface displaying varying combinations of topographic features, mechanical and adhesive properties. Firstly, hMSCs were cultivated on nanograted PDMS substrates with 350 nm wide ridge, 100 nm high (0.7  $\mu\text{m}$  pitch) or on 700 nm wide ridge, 250 nm high (1.4  $\mu\text{m}$  pitch) (Fig. 1) with equal adhesive (plasma treated, PT) and mechanical properties (1.5 MPa).

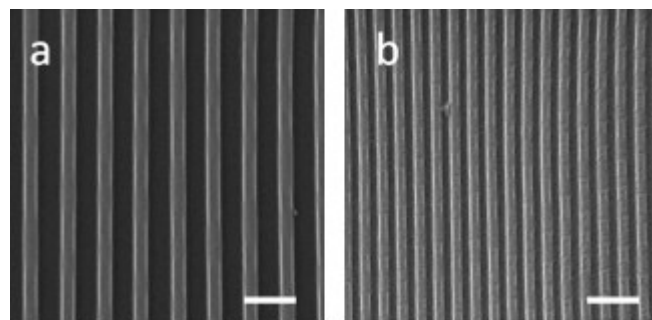


**Figure 1:** SEM images of PDMS nanopatterned substrates (a) substrate with 1.4  $\mu\text{m}$  pitch, 700 nm ridges and 700 nm grooves. (b) substrate with 0.7  $\mu\text{m}$  pitch, 350 nm ridges and 350 nm grooves. Scale bar 2  $\mu\text{m}$ .

In both conditions, at 24 h cells exhibited a strong polarization along the pattern direction and at 48 h post seeding proliferated and migrated preferentially along it (Fig. 2).

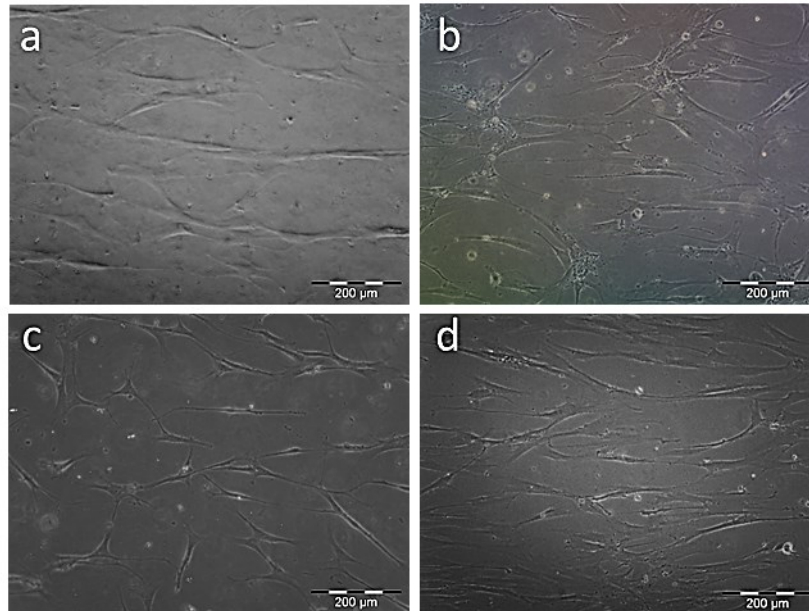


**Figure 2:** bright field images of MSCs cultured on 0.7  $\mu\text{m}$  pitch at (a) 24 h and (b) 48 h post seeding and on 1.4  $\mu\text{m}$  pitch at (c) 24 h and (d) 48 h post seeding

After 1 week of culture hMSCs self-organized in the form of cell monolayers on both substrates. Cell cytoskeleton and nucleus perceived the topographic signal and acquired an elongated shape perfectly parallel to the substrate nanogrooves. In addition, the MSCs inside the aligned sheets migrated in the same direction of the topographic pattern. This observations were confirmed by time lapse video showing that the MSC population is assembled in an aligned multilayer, and it is possible to discern individual cell migrating along pattern direction (Fig. 3).

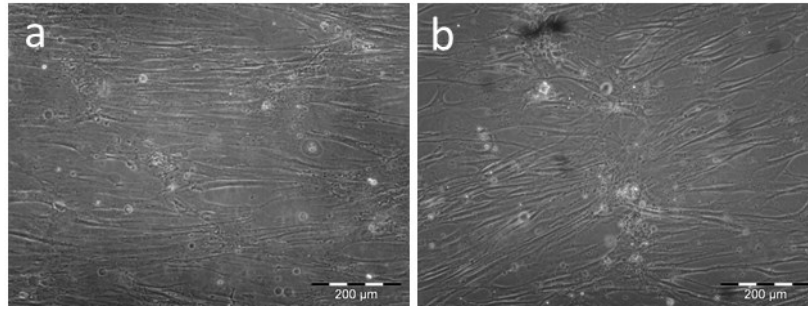


**Figure 3:** bright field images of MSCs cultured on (a) 0.7  $\mu\text{m}$  pitch and (b) 1.4  $\mu\text{m}$  pitch pattern at 1 week post seeding

A closer inspection of cellular and matricellular components revealed that MSCs were able to assemble a thin 3D sheet within 1wk. The sheets were composed of densely packed and aligned fibronectin matrix, but with scarce presence of collagen fibers (Fig. 4).

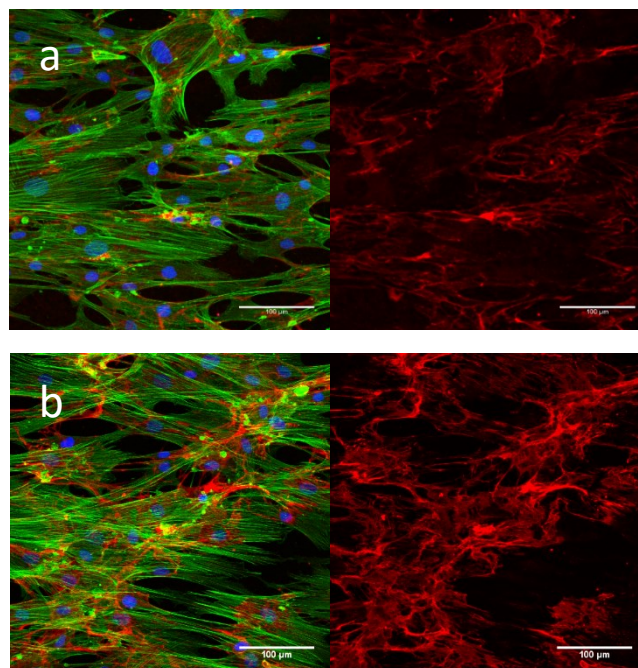


**Figure 4:** Confocal images of cytoskeleton assemblies (green), nuclei (blue) and fibronectin (red) in hMSCs monolayer cultivated for 7 days on oxygen plasma treated (a) 0.7  $\mu\text{m}$  pitch pattern and (b) 1.4  $\mu\text{m}$  pitch pattern.

In order to increase and stabilize the neo-synthesized collagen by MSCs, medium was supplemented with ascorbic acid after 7 days of culture; furthermore, ascorbic acid plays a crucial role in cell proliferation [14] and cell sheet formation [15].

After 15 days of cultures, hMSCs spontaneously formed dense cell multilayers with a high degree of cell alignment and polarization with respect to the direction of nanopattern. At 20 day post seeding the multilayers appeared as a 3D supracellular constructs in which collagen and fibronectin fibers were more mature and densely packed and strongly aligned to the pattern direction.

Despite these morphological evidences, time lapse observation of the hMSC self-organization and cell multilayer formation revealed that cells assemble in different structures according to the substrate features. In more detail, the excessive spreading of cells on the 1.4  $\mu\text{m}$  pitch pattern cause a lower cell motility compared to that generated by the cells on the 0.7  $\mu\text{m}$  pitch pattern (Fig. 5). In particular, MSCs cultured on 0.7  $\mu\text{m}$  pitch PT pattern were able to create more uniform and homogenous tissue probably because of the optimal balance between cell adhesion and cell remodeling.

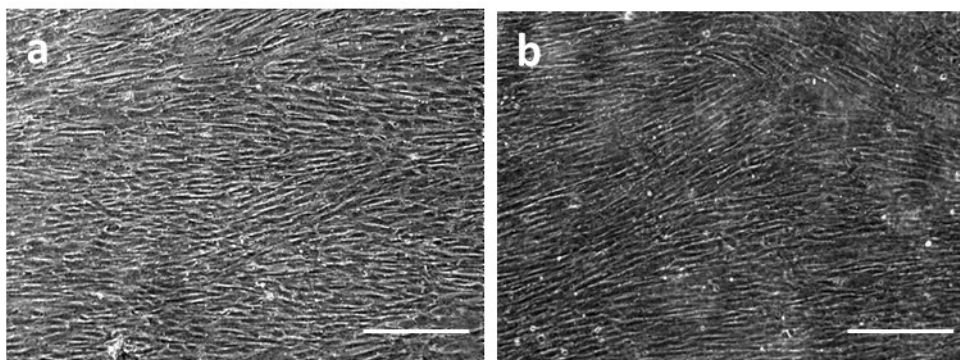


**Figure 5:** bright field images of MSCs cultured on (a) 0.7  $\mu\text{m}$  pitch and (b) 1.4  $\mu\text{m}$  pitch patten at 20 days post seeding. Scale bar 200  $\mu\text{m}$ .

These peculiar dynamics suggested that, in order to control the self-organization processes by modulating the material features, it is crucial to consider adhesion and

cell-generated forces as two intimately connected phenomena, essential for cell survival, proliferation and migration.

Moreover, cell proliferation of hMSCs on the two nanotopographic patterns was not significantly different suggesting that the topographic signal we exploited does not affected the proliferative ability of this type of cells but only their self-organization.

Confocal microscopy of cytoskeleton assembly, nuclei, fibronectin and collagen in 3D structures of hMSCs on 0.7  $\mu\text{m}$  pitch patterned substrate and on 1.4 pitch patterned substrate treated with oxygen plasma after 2 week culture, displayed a dense fibronectin and collagen matrix but only the 0.7  $\mu\text{m}$  pitch pattern promoted a uniform deposition of matrix (Fig. 6).

Owing to these characteristics we decided to focus further investigations on the tissues generated on the 0.7  $\mu\text{m}$  pitch PT patterns only.

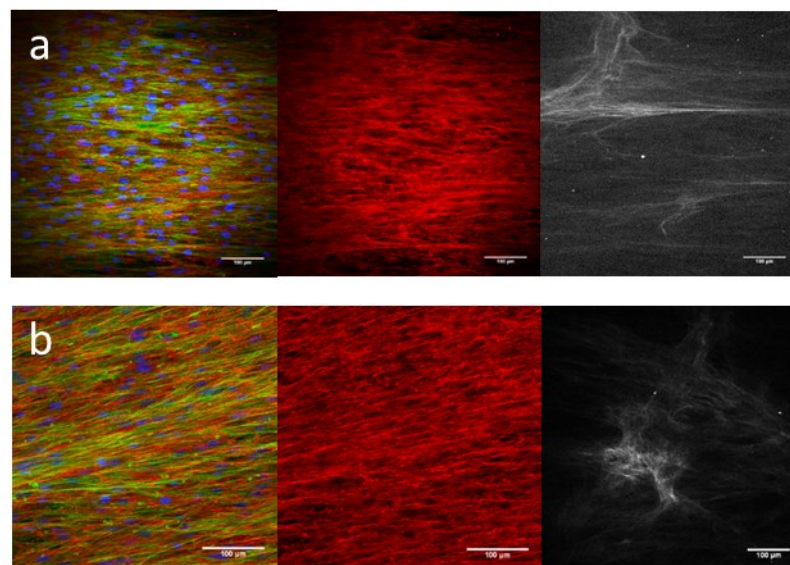


**Figure 6:** Confocal images of cytoskeleton assembly (green), nuclei (blue), fibronectin (red) and collagen SHG signals (grey) in hMSCs multilayer cultivated for 20 days on oxygen plasma treated (a) 0.7  $\mu\text{m}$  pitch pattern and (b) 1.4  $\mu\text{m}$  pitch pattern.

### 2.2.2 Effect of substrate stiffness on hMSCs self-organization

The initial condition of cell adhesion on the substrate profoundly impact cell self-organization and tissue formation. Within this context, it is well recognized that the mechanical stiffness of the substrate dramatically affects cell adhesion and dynamics [16]. Therefore, we asked whether the mechanical properties of the substrate might synergistically act with topography to alter cell self-organization and tissue structure. hMSCs were seeded on plasma treated 0.7  $\mu\text{m}$  pitch pattern substrates, fabricated by varying the prepolymer base to curing agent ratio: 10:0.5 (SOFT  $\sim$  0.74 MPa), 10:1 (MEDIUM  $\sim$  1.23 MPa) and 10:2 (HARD  $\sim$  2.53 MPa).

After 1 week of culture, hMSCs perceived the nanogrooves and showed the actin stress fibers aligned with pattern direction, also cell nuclei were polarized along the nanopattern direction (Fig 7). Time lapse video highlighted that the combinatorial effects of substrate topography and adhesivity resulted in a migratory behavior of hMSCs parallel to the pattern direction (data not shown). These orchestrated movements allowed the production and remodeling of a matrix displaying a high degree of alignment.

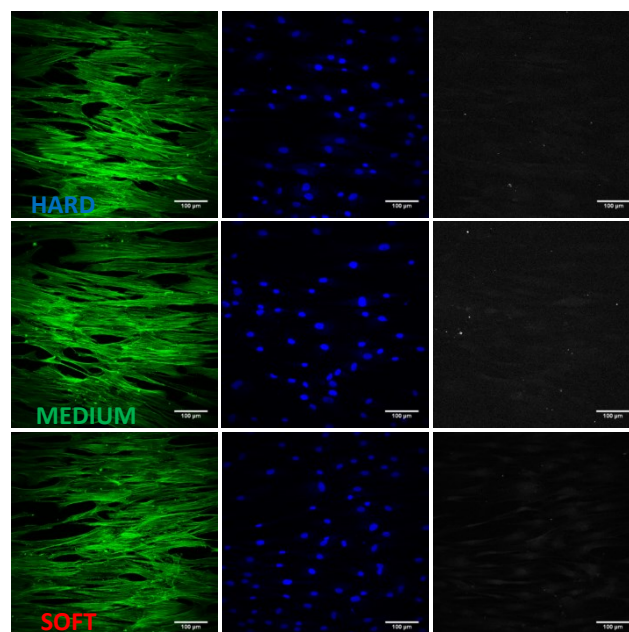


**Figure 7:** Confocal images of cell sheets derived from hMSCs cultivated for 7 days on hard, medium and soft oxygen plasma treated 0.7  $\mu\text{m}$  pitch patterned PDMS. The actin bundles were stained with phalloidin (green), and nuclei with sytox (blue). In grey, SHG images of the collagen fibers.

Also in this case, ascorbic acid was added to the culture medium after 1 week to stimulate and stabilize collagen production. At this time of culture dramatic differences of cell morphology mediated by substrate stiffness were not evident. Furthermore, the migration and proliferation speed appeared comparable in all experimental conditions.

On day 15, as a result of cell proliferation and remodeling, the nanopatterns were populated by a dense cell sheet multilayers inside of which the hMSCs were immersed in a matrix rich in collagen as showed by the images obtained by SHG (Fig. 8). In particular, aligned collagen fibers became clearly visible from day 10 (data not shown).

These observations allowed us to obtain information on the positioning of cells and their interplay with fibronectin and collagen fibrils.

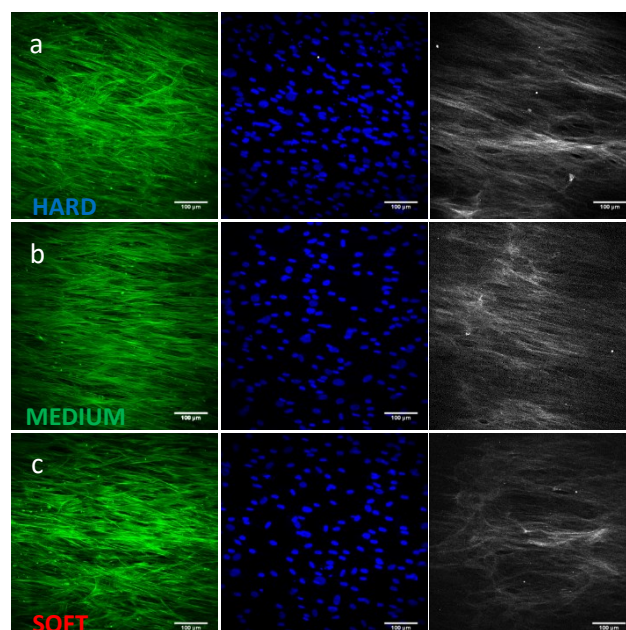


**Figure 8:** *Confocal images of cell sheets derived from hMSCs cultivated for 15 days on hard, medium and soft oxygen plasma treated 0.7  $\mu\text{m}$  pitch patterned PDMS. The actin bundles were stained with phalloidin (green), and nuclei with sytox (blue). In grey, SHG images of the collagen fibers.*

Z-stacked confocal images of 15 day old samples stained with phalloidin and sytox green showed some differences in terms of cell multilayers composition between the substrates with different degree of stiffness. In more detail, on PDMS with intermediate stiffness, the hMSCs migrated and proliferated following the nanogrooves direction and the collagen and fibronectin fibrils formed dense matrix (Fig 8b). This matrix assume the same direction of the cells body, by acting as endogenous scaffolds with the same topographic features of underlying PDMS.

In this way, the hMSCs located on the top of multilayer perceived the same topographical signals of cells still in contact with the PDMS surface and the whole developed tissue resulted highly densely packed and homogeneous.

Conversely, on hard and soft PDMS substrates, the cells showed different behavior. Also in these conditions in the early stages of culture, the topography, together with the oxygen plasma treatment, promoted the cell attachment and spreading along the direction of the nanopattern grooves. However, after 15 days of culture we observed the formation of dense cell-matrix multilayer with high level of heterogeneity in collagen, fibronectin and cell positioning (Fig 8a-c). In more details the cell and matrix located on the upper layer of sheets showed a different orientation compared with cell and matrix positioned at the bottom of the multilayer.

In these conditions the cells located in the upper layers proliferated losing the initial alignment imposed by nanopattern grooves.

In summary, the self-organized multilayer developed on hard and soft nanograted PDMS show similarity in terms of heterogeneity in the spatial arrangement of cells and collagen fibers.

Altogether these data suggest that the initial biochemical/biophysical signals of the material surface affect adhesion and morphology, but also matrix production and assembly. Once produced, the matrix provides cells with additional signals, which soon end up in establishing a dynamic reciprocity between cells and matrix, i.e. cells perceive the matricellular signals and the matrix is remodelled by cells. Therefore the structure of the tissue and the behavior of cells are the result of a continuous process of interplays and feedbacks.

### *2.2.3 Scanning Electron Microscopy (SEM) analysis*

SEM examinations were performed to analyse the interplay between hMSCs and the novo synthesized matrix.

The observations of aligned tissues, developed on plasma treated 0.7  $\mu\text{m}$  pitch pattern substrates, showed cells closely packed in the form of sheets parallel to the pattern direction (Fig. 9). The examination of the upper regions of tissues surface revealed a highly aligned and homogeneous cell layer, although mismatched to the direction of the underlying pattern, regardless of the level of rigidity of PDMS substrates. In more detail, while all the substrates promoted the formation of collagen and fibronectin rich sheets, substrates with medium stiffness induced higher degree of cell and matrix alignment along with a more uniform collagen deposition. Moreover, hMSCs were well aligned to the pattern direction on the whole area of the sample preserving the initial topographic signal imposed by the substrate.

Furthermore, we focused the attention on the extracellular matrix composition; in the intercellular regions, we observed some recesses rich in densely packed collagen-fibronectin matrix.

The effect of surface stiffness arose from the different distribution and arrangement of the matrix produced. Indeed, soft surfaces were constituted of more sporadic of thick and well defined collagen fibers.

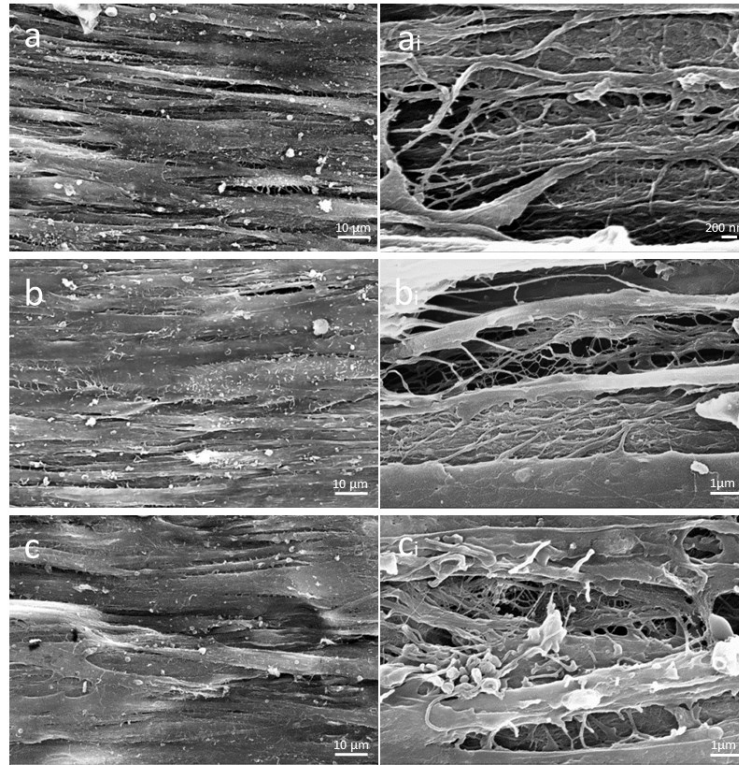


**Figure 9.** SEM images of hMSC cell sheets formed on (a) HARD, (b) MEDIUM and (c) SOFT PT 0.7  $\mu\text{m}$  pitch PDMS and correlate fibronectin and collagen matrix structures ( $a_i$ ,  $b_i$ , and  $c_i$ )

The results of these observations seem to confirm the morphological analysis performed by means of multiphoton microscopy. The combinatorial effect of topographic and mechanical properties of substrates in the three different conditions resulted in the production of aligned and packed 3D tissues that probably differed in the amount and distribution of extracellular matrix network.

#### *2.2.4 Molecular profile analysis of hMSC constituting cell sheets*

Lineage specification of native stem cells induced by soluble stimuli has been well described for in vitro models [17, 18]. In vivo, the behaviour of stem cells, is crucially influenced by their interactions with a plethora of biochemical and biophysical signals provided by niche components, which underline the pivotal role of the microenvironment in regulating stem cell specification. For instance, hMSCs actively sense the mechanical properties of their environment to differentially commit to osteogenic, myogenic or neuronal lineages depending on the elasticity of their substrates [11, 19].

Owing to the differences in cell morphology, and matrix arrangement observed on the three substrates, we asked whether such differences could impact on hMSC lineage specification. To this aim, we analysed the expression of stemness, pluripotency, matrix and differentiation markers on multilayer cell sheets obtained, after 20 days of culture without the addition of differentiating medium, by Real Time-PCR analysis (RT-PCR).

The results indicate that at 20 days the expression of stemness markers (CD29, CD44, CD73, CD90, CD105) in hMSC cell sheets obtained on plasma treated 0.7  $\mu\text{m}$  pitch pattern was higher with respect to wide type hMSCs at time 0 ( $t_0$ ), which were not exposed to either topographic or mechanical signals (Fig. 10a), except for the expression of CD105 that showed a low expression in all samples. Interestingly, an higher expression level of these markers were detected in the cell sheets obtained on substrates with intermediate stiffness (CD29 6-fold, CD44 5-fold, CD73 3-fold, CD90 6-fold significantly higher). In contrast, hMSC cell sheets obtained on flat PDMS surfaces showed expression levels similar to that of wild type cells (Fig.10b).

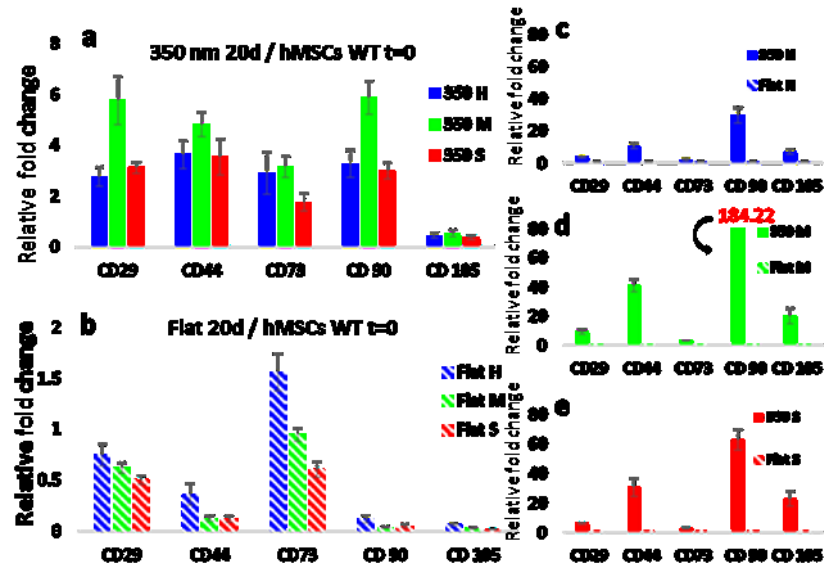


**Figure 10:** Gene expression of stemness markers including CD29, CD44, CD73, CD90 and CD105 in hMSC cell sheets after 20 days culture on (a) 0.7  $\mu\text{m}$  pitch pattern PDMS substrates and on (b) flat PDMS substrates treated with oxygen plasma. (C), (d) and (e) the ratio between the gene expression levels of the cell sheets developed on nanopatterned substrate and those in the cell sheet products on the flat substrate. Relative gene expression was quantified using the  $2^{-\Delta\Delta\text{CT}}$  method by normalizing the target gene expression to GAPDH and reported in histograms as relative fold change.

Furthermore, we compared the expression of genes involved in stemness phenotype in hMSC seeded on nanopatterned substrates and on FLAT surfaces (Fig. 10c-e). We found that the expression of the stemness markers was higher in monolayers developed on nanopatterned substrates with medium level of stiffness compared with the cells seeded on FLAT surface, with the same degree of rigidity (Fig. 10d). Therefore, both topography and substrate stiffness are responsible for the generation of a 3D tissue that preserves the stemness signature.

The expression of pluripotency- associated genes was significantly up-regulated after 20 days of culture in hMSC cell sheets obtained on plasma treated 0.7  $\mu\text{m}$  pitch pattern compared to hMSCs wilde type (Oct 3/4 6,15- fold, Nanog 3,7-fold, Klf4 2,5-

fold, Sox2 2,5-fold) (Fig. 11a). In particular the maximal up-regulation was reached in the cell sheets obtained on intermediate PDMS. On flat surfaces the relative mRNA levels were mainly down-regulated compared to those expressed in hMSCs t0 (Figure 11b). These data indicated that in absence of the optimal set of initial conditions namely a fine combination of topographic and mechanical signals, after 20 days of culture hMSCs multilayers were a result of an heterogeneous population in which only a little part of cells maintained the stemness profile.

By comparing the expression levels in the cell sheets developed on nanopatterned substrates and those in the cell sheets obtained on the flat substrates, with the same level of rigidity, we observed an evident up regulation in MSC sheets developed on plasma treated 0.7  $\mu\text{m}$  pitch pattern (Figure 11c-e).

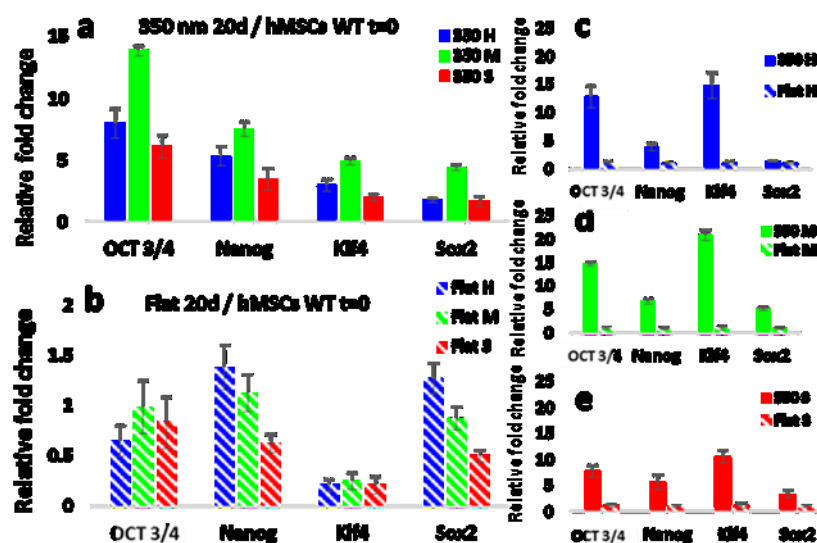


**Figure 11:** Gene expression of pluripotency markers including OCT 3/4, Nanog, Klf4 and Sox2 in hMSC cell sheets after 20 days culture on (a) 0.7  $\mu\text{m}$  pitch pattern PDMS substrates and on (b) flat PDMS substrates treated with oxygen plasma. (C), (d) and (e) the ratio between the gene expression levels of the cell sheets developed on nanopatterned substrate and those in the cell sheet products on the flat substrate.

The evidence of the over-expression of pluripotency markers on nanopatterned substrates with the intermediate stiffness suggested that the combined effect of topographic signals and mechanical properties generated a microenvironment that supported not only the maintenance of a preexisting stemness of hMSCs, but was able to activate a sort of process of reprogramming towards a pluripotency state.

Next we investigated the expression of matrix-associated genes in cell sheets developed on patterned substrates and on flat surfaces. These were analysed compared to hMSCs cultivated on Petri dish for 20 days.

The relative expression of such genes in the cells grown on 0.7  $\mu\text{m}$  pitch pattern at 20 days was higher with respect to hMSCs cultivated on Petri dishes for the same time (Collagen 1 5,7-fold, Collagen 2 4,7-fold, Collagen 3 4,6-fold, Fibronectin 6,9-fold and Decorin 2,3-fold higher) (Fig. 12a).

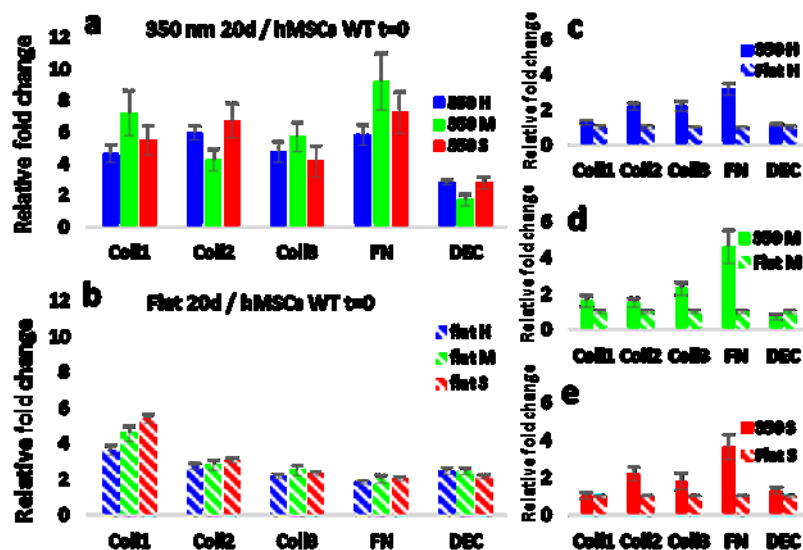


**Figure 12.** Gene expression of matrix markers including collagen type 1, collagen type 2, collagen type 3, fibronectin and decorin in hMSC cell sheets after 20 days culture on (a) 0.7  $\mu\text{m}$  pitch pattern PDMS substrates and on (b) flat PDMS substrates treated with oxygen plasma. (c), (d) and (e) the ratio between the gene expression levels of the cell sheets developed on nanopatterned substrate and those in the cell sheet products on the flat substrate.

In this a clear correlation between the expression of matrix markers and the material stiffness was not observed. On flat PDMS, we observed slight increase of the expression levels of matrix markers compared with those of hMSCs cultivated on Petri dishes (Fig. 12b), suggesting that, although the absence of a topographic signals, the PDMS mechanical properties stimulated a higher production of the extracellular matrix respect to the Petri dishes. When we compared the expression levels of matrix markers in the cell sheets developed on nanopatterned substrates and those in the cell sheets obtained on the flat substrates, with the same degree of stiffness, we observed an higher level of expression on nanopatterned substrates (Fig. 12c-e). Probably this behavior was the result of the influence of the topographic signal not only on the stimulation of matrix formation, but also on the structural organization of the de novo ECM within the multilayer tissues.

Finally, we complemented this analysis with the expression of genes involved in the tenogenic (TNMD, tenomodulin and Scx, scleraxis), myogenic (Myogenin and Myf 5, Myogenic factor 5), osteogenic (RunX2 and OC, Osteocalcin F) and chondrogenic (ACAN, aggrecan, Coll2 $\alpha$ , SOX9 and Comp1) differentiation. The analysis was performed in cell sheets obtained on nanopatterned substrates (Fig. 13a), on flat surfaces (Fig 13b) and in hMSCs cultivated on Petri dish (Fig. 13c), we found that the relative mRNA levels were strongly downregulated with respect to the baseline levels of the GAPDH housekeeping gene, with values near to zero.

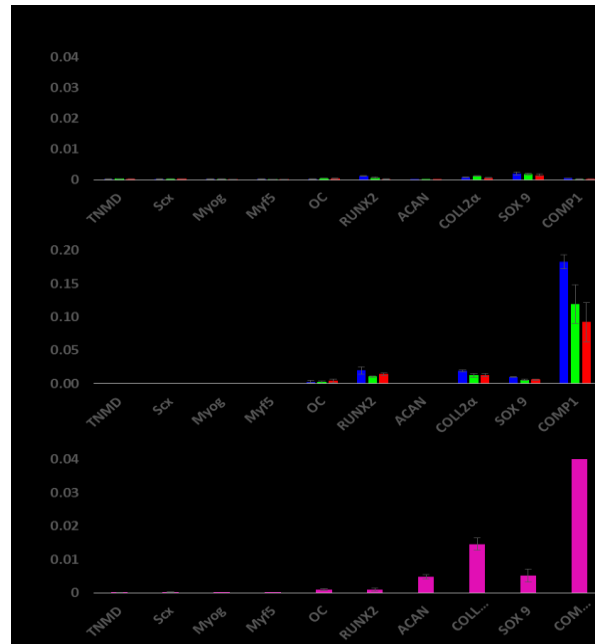


**Figure 13.** Gene expression of tenogenic differentiation (TNM; Scx), myogenic (Myf5; Myogenin), osteogenic (RunX2; OC) and chondrogenic (ACAN; Col2α; Comp1; Sox9) differentiation markers in hMSC cell sheets after 20 days culture on (a) 0.7 μm pitch pattern PDMS substrates, on (b) flat PDMS substrates treated with oxygen plasma and in (c) hMSCs cultivated on Petri dish.

Taken together molecular profiles of 3D tissues, resulted from the combinatorial effect of biophysical and biochemical signals, confirmed our morphological observations. In particular, after 20 days of culture the plasma treated 0.7 μm pitch pattern with intermediate stiffness guided the hMSC behaviour along the formation of microenvironment that affected MSC fate leading to the retention and enhancement of stemness and pluripotency properties.

In this work, we demonstrated the central role of physical cues such as topography and rigidity on the cell adhesion control that culminates in the in vitro generation of self-organized hMSCs cell sheet, rich in highly aligned matrix, without the employment of growth factors or exogenous scaffold matrices.

While the effect of nanopatternig on cell adhesion and differentiation has been widely investigated in the context of isolated cells, its influence of the spatial arrangement of cells and de novo synthesized matrix is still poorly explored.

Native tissues are endowed with a highly organized nanofibrous ECM which plays a critical role in providing mechanical support, directing cell ad growth, as well as regulating development, homeostasis and regeneration. Different nanopatterned substrates have been employed to mimic the nanotopography of natural ECM for a wide range of tissue engineering studies but most of these nanoscale scaffolds are fabricated by synthetic materials which fail to adequately mimic the composition of natural ECM [20].

In order to replicate the chemical and biological motifs of the ECM found in natural tissues [21], researchers have adopted the approach of fabricating nanofibrous materials from cultured cells in vitro. Xing et al. [22] produced a uniform and highly nanofibrous natural ECM scaffold from a human dermal fibroblast cell sheet grown on synthetic nanogratings for 8 weeks. A highly organized ECM scaffold was obtained by decellularizing the fibroblast cell sheet. The capability of the aligned nanofibrous natural ECM scaffold in directing and supporting cell alignment and growth was tested by re-seeding human MSCs (hMSCs), which showed good alignment and active proliferation. The applications of cell-derived ECM as a physiologically functional source of the complex set of naturally occurring bioactive signals has gained increasing interest. The development of highly organized engineered ECM scaffolds is crucial to create biomimetic tissues since native tissues are highly organized. Furthermore, mimicking the complexity of ECM and cell organization it is possible to avoid the problems of pathogen transfer and host immune response [23]. For all these reasons, the aligned nanofibrous ECM scaffold holds great potential in engineering organized tissues.

In addition to topographic signals, we demonstrated that material stiffness is also effective in influencing the MSC self-assembly and fate. In more details, we reported that on a substrate with intermediated stiffness, hMSCs generate a cell sheet with a higher degree of homogeneity in terms of cell and ECM fibers aligned. Substrate rigidity also impacts gene expression suggesting that intermediate PDMS stiffness improves stemness maintenance, enhances pluripotency and prevents differentiation. Probably, the signals provided by the tissue microenvironment regulates stem cell self-renewal in culture. In this context, Gilbert et al. [24] reported that unlike isolated muscle stem cells (MuSCs) cultured on rigid plastic dishes ( $\sim 10^6$  kPa), MuSCs cultured on soft hydrogel substrates that mimic the elasticity of muscle (12kPa) self-renew in vitro and contribute extensively to muscle regeneration when subsequently transplanted into mice. Their molecular results showed that soft substrates enhance MuSC survival, prevent differentiation and promote stemness. Studies employing biomimetic culture platforms will broadly impact stem cell studies by facilitating in vitro propagation while maintaining stemness and the capacity to regenerate tissues, a critical step towards the development of cell-based therapies.

### **2.3 Conclusions**

Shape and functions of tissues and organs is the results of a continuous and mutual interplay between cells and matrix. During the development process cells perceive biochemical and biophysical cues of the microenvironment and transduce them into intracellular signals that guide and control cell growth, differentiation and migration that are of fundamental relevance during morphogenesis. For example, fate decision of stem cells is regulated in response to a complex array of biochemical and biophysical signals from their niche.

Here, we have demonstrated that mechanical and topographic properties of culturing substrates act in concert to guide MSC self-organization and tissue formation.

We used nanopatterned substrates able to control and guide hMSC behaviour to generate ordered tissue in vitro. In particular we show that by changing the combination of the initial conditions we obtain different behaviours in terms of cell-self-organization and tissue development.

Decreasing the pattern features from 1.4  $\mu\text{m}$  to 0.7  $\mu\text{m}$  pitch and improving the adhesion via oxygen plasma treatment that increase the hydrophilicity, the cell behavior was dramatically altered. In more details, we observed the development of homogeneous tissues with a high degree of cellular and matrix alignment. The combinatorial effect of these substratum properties were shown to regulate the formation of hMSC cell sheets and influence subsequent tissue development. Molecular analyses suggest that such conditions create a microenvironment permissive for stemness retention and upregulation of pluripotency genes. In conclusion, our results demonstrate that both the substrate chemical/physical features and the characteristics of the de novo synthesized matrix dramatically affect cell fate and tissue functions. Therefore, nanoengineered materials surfaces can be in principle employed to set off the hMSC program toward tissue genesis in a deterministic manner by using the correct combination of initial biophysical signals. All together, these results present an in vitro model system that can be used to produce tissues for studying the self-renewal and the differentiation ability of hMSCs or to direct the development of differentiated tissues on which to test new drug molecules.

## 2.4 References

1. Zhu, B., Zhang, Q., Lu, Q., Xu, Y., Yin, J., Hu, J. & Wang, Z. (2004) "Nanotopographical guidance of C6 glioma cell alignment and oriented growth". *Biomaterials* 25.
2. Engler AJ, Sen S, Sweeney HL, Discher DE (2006) "Matrix elasticity direct stem cell lineage specification". *Cell*, 126.
3. Dalby MJ, Gadegaard N, Tare R, Andar A, Riehle MO, Herzyk P, Wilkinson CD, Oreffo RO. The control of human mesenchymal cell differentiation using nanoscale symmetry and disorder. *Nat Mater.* 2007; 6:997-1003.
4. Yim EK, Pang SW, Leong KW. Synthetic nanostructures inducing differentiation of human mesenchymal stem cells into neuronal lineage. *Exp Cell Res.* 2007, 313:1820-1829.
5. Gjorevski N, Ranga A, Lutolf MP. Bioengineering approaches to guide stem cell-based organogenesis. *Development.* 2014;141:1794-804.
6. Beloussov LV, Louchinskaia NN, Stein AA. Tension-dependent collective cell movements in the early gastrula ectoderm of *Xenopus laevis* embryos. *Dev Genes Evol.* 2000; 210:92-104.
7. Huang S, Ingber DE. The structural and mechanical complexity of cell-growth control. *Nat Cell Biol.* 1999; 1:E131-8.
8. Ingber DE, Madri JA, Jamieson JD. Neoplastic disorganization of pancreatic epithelial cell-cell relations. Role of basement membrane. *Am J Pathol.* 1985;121:248-260.
9. Rozario T, DeSimone DW. The extracellular matrix in development and morphogenesis: a dynamic view. *Dev Biol.* 2010 ;341:126-140.
10. Vogel V, Sheetz MP. Cell fate regulation by coupling mechanical cycles to biochemical signaling pathways. *Curr Opin Cell Biol.* 2009;21:38-46.

11. Engler AJ, Sen S, Sweeney HL, Discher DE. Matrix elasticity directs stem cell lineage specification. *Cell*. 2006 ;126:677-89.
12. Rowlands AS, George PA, Cooper-White JJ. Directing osteogenic and myogenic differentiation of MSCs: interplay of stiffness and adhesive ligand presentation. *Am J Physiol Cell Physiol*. 2008, 295,1037-1044.
13. Natale CF, Ventre M, Netti PA. Tuning the material-cytoskeleton crosstalk via nanoconfinement of focal adhesions. *Biomaterials*. 2014, 35, 2743-2751.
14. Choi K. M., Y. K. Seo, H.H. Yoon, K.Y. Song, S.Y. Kwon, H.S. Lee, et al. Effect of ascorbic acid on bone marrow-derived mesenchymal stem cell proliferation and differentiation, *J. Biosci. Bioeng*. 2008, 105, 586-594.
15. Wei F, Qu C, Song T, Ding G, Fan Z, Liu D, et al. Vitamin C treatment promotes mesenchymal stem cell sheet formation tissue regeneration by elevating telomerase activity, *J. Cell. Physiol*. 2012, 227, 3216-3224.
16. Wang N, Tytell JD, Ingber DE. Mechanotransduction at a distance: mechanically coupling the extracellular matrix with the nucleus. *Nat Rev Mol Cell Biol*. 2009; 10:75-82.
17. Gang EJ, Jeong JA, Hong SH, Hwang SH, Kim SW, Yang IH, Ahn C, Han H, Kim H. Skeletal myogenic differentiation of mesenchymal stem cells isolated from human umbilical cord blood. *Stem Cells*. 2004; 22:617-624.
18. McBeath R, Pirone DM, Nelson CM, Bhadriraju K, Chen CS. Cell shape, cytoskeletal tension, and RhoA regulate stem cell lineage commitment. *Dev Cell*. 2004; 6:483-495.
19. Gilbert PM, Havenstrite KL, Magnusson KE, Sacco A, Leonardi NA, Kraft P, Nguyen NK, Thrun S, Lutolf MP, Blau HM. Substrate elasticity regulates skeletal muscle stem cell self-renewal in culture. *Science*. 2010; 329:1078-81.
20. Badylak SF, Freytes DO, Gilbert TW. Extracellular matrix as a biological scaffold material: Structure and function. *Acta Biomater*. 2009; 5:1-13.

21. Reing JE, Zhang L, Myers-Irvin J, Cordero KE, Freytes DO, Heber-Katz E, Bedelbaeva K, McIntosh D, Dewilde A, Braunhut SJ, Badylak SF. Degradation products of extracellular matrix affect cell migration and proliferation. *Tissue Eng Part A*. 2009; 15:605-14.
22. Xing Q, Vogt C, Leong KW, Zhao F. Highly Aligned Nanofibrous Scaffold Derived from Decellularized Human Fibroblasts. *Adv Funct Mater*. 2014; 24:3027-3035.
23. Lu H, Hoshiba T, Kawazoe N, Koda I, Song M, Chen G. Cultured cell-derived extracellular matrix scaffolds for tissue engineering. *Biomaterials*. 2011; 32:9658-66.
24. Gilbert PM, Havenstrite KL, Magnusson KE, Sacco A, Leonardi NA, Kraft P, Nguyen NK, Thrun S, Lutolf MP, Blau HM. Substrate elasticity regulates skeletal muscle stem cell self-renewal in culture. *Science*. 2010; 329:1078-81.

### **3. Engineered material surfaces to control tissueogenesis**

#### **3.1 Introduction**

Morphogenetic events are launched by initial conditions defined by the physicochemical characteristics of the environment. The sequence of processes that occurs afterward propagates with an astonishing consistency and terminates with the establishment of highly complex tissue structures. During the last decades, much effort was dedicated to unravel the mechanisms behind morphogenesis with the belief that these would have suggested inspiring strategies to tackle unsolved problems such as the treatment of degenerative pathologies and the replacement of injured tissues. Major breakthroughs in this field have recently regarded the in vitro development of organoids such as brain, intestine, and optic-cup [1–3], which paved the way for the use of organoids systems as developmental and disease models or for drug screening [4,5]. These studies rely on the spontaneous spatial self-organization and differentiation of embryonic stem cells (ESCs) or induced pluripotent stem cells (iPSs) spheroids, which if cultivated in specific conditions, mostly in low attachment or suspension, evolve in complex assemblies displaying remarkable structural and molecular similarities with native tissues and organs. However, very little is known on the influence of the initial physical interactions with the surrounding environment on the morphogenetic process. For instance, the physical properties of the supporting extracellular matrix (ECM) in the form of microstructure and stiffness are known to control and guide specific morphogenetic events [6]. It is therefore possible that exogenous physical stimuli might control and guide the self-organization process, thus providing an adequate microenvironment, which eventually dictates form and functions of supracellular structures. In particular, FAs are the mechanical links with the extracellular environment and are mainly responsible for the outside-in and inside-out transmission of forces [7]. These forces not only are crucial for the

establishment of the tissue morphology but also regulate cell differentiation through specific mechanotransduction pathways [8]. Indeed, several studies exploiting material surfaces able to modulate cell contractility through FA formation and growth demonstrated that physical signals potently control cell fate and functions [9–11]. However, these studies provided little insight into the role of FA formation and cell generated forces on tissue formation.

Our hypothesis is that by exploiting material surface nanopatterning it is possible to control the initial spatial positioning and growth of FAs that ultimately dictate tissue formation: from cell self-organization down to differentiation in a deterministic manner.

The aim of the work reported in this chapter is to show that surface nanopatterning can control the initial assembly of focal adhesions, hence guiding hMSCs through the process of self organization and differentiation. This process self-sustains, leading to the development of macroscopic tissues with molecular profiles and microarchitecture reminiscent of embryonic tendons. Therefore, material surfaces can be in principle engineered to set off the hMSC program toward tissueogenesis in a deterministic manner by providing adequate sets of initial environmental conditions. In more details, hMSCs, cultivated on PDMS substrates with arrays of parallel channels having 700 nm width and 1.4  $\mu\text{m}$  pitch without exogenously added growth factors, are guided through the process of self- organization and differentiation, which led to the development of 3D tissues with cellular and extracellular matrix organization closely resembling that of an embryonic human tendon.

## **3.2 Results and discussion**

### *3.2.1. Single and collective cell dynamics*

To investigate the effect of surface topography on cell behaviour, hMSCs were cultivated on nanograted PDMS substrates with 700 nm wide ridge, 250 nm high (1.4

$\mu\text{m}$  pitch) or on flat PDMS substrates with equal adhesive (treatment with serum proteins) and mechanical properties (1.5 MPa).

First, cells seeded at low density on the patterned surface exhibited a strong polarization along the pattern direction and migrated preferentially along it (Fig. 1a, b). On day 3 postseeding, hMSCs formed cell aggregates oblong in shape and with the long axis predominantly directed perpendicularly to the pattern (Fig. 1a, b). From day 3 to day 6, the scattered aggregates gathered and merged forming elongated structures (Fig. 1a, b). A considerable recruitment of cells within the structures was observed from day 6.

This caused the structures to become thicker and densely populated and a concurrent structure straightening was observed in this time frame. On day 7, several long and straight structures were visible on the nanopatterned surface. Furthermore, cells within the structures were clearly located on different planes, thus forming a 3D cylindroid. Such a cellular assembly suggested the existence of a provisional scaffolding matrix. Indeed, hMSCs are known to synthesize collagen *in vitro* [12] and to retain the collagen produced culture medium was supplemented with ascorbic acid. Interestingly, ascorbic acid supplemented at day 0 did not allow the formation of the long and straight supracellular structures. From day 7 onward, the structures kept growing owing to cell recruitment from the surroundings or the merging of two sufficiently close structures. On day 15, the nanopattern was mostly populated by macroscopic, cylindrical structures (Fig. 1c).

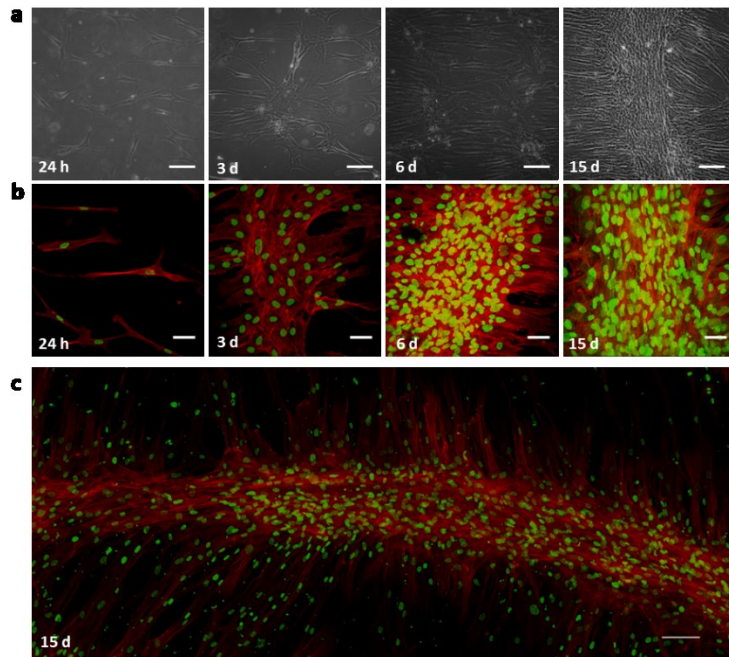


**Figure 1:** (a) brightfield images and (b) confocal images of hMSCs cultivated on the 1.4  $\mu\text{m}$  pitch pattern at 24h, 3d, 6d and 15d post seeding. (c) Confocal tile scan of tendon-like structure after 15 days of culture on the 1.4  $\mu\text{m}$  pitch patterned substrate. Scale bar is 100  $\mu\text{m}$  in panels a and c and 50  $\mu\text{m}$  in panel b.

Conversely, the hMSCs seeded on a flat surface displayed neither a macroscopic alignment, nor a directed migration (Fig. 2). From day 1 to day 3, the flat surface induced the formation of spherical cell aggregates that occasionally fused together (Fig. 2). However, such cell aggregates never developed into ordered supracellular structures.

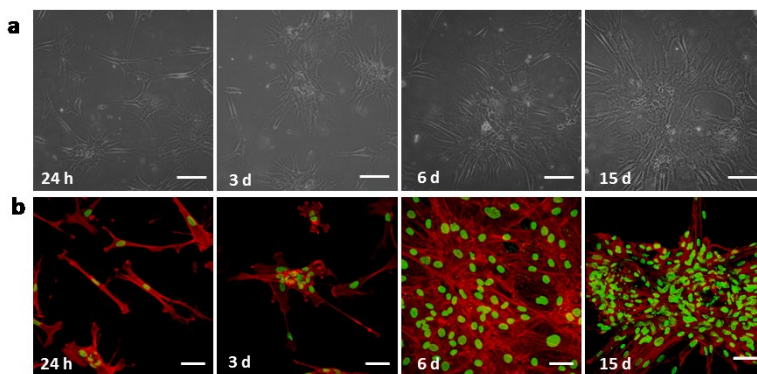


**Figure 2:** (a) brightfield images and (b) confocal images of hMSCs seeded on flat surfaces at 24h, 3d, 6d and 15d post seeding. Scale bar is 100  $\mu\text{m}$  in panel a and 50  $\mu\text{m}$  in panel b.

This peculiar dynamics suggested the hypothesis that the modulation of FA growth and spatial positioning mediated by the nanopattern controls the cytoskeletal assembly of the cell at the initial adhesion stage that in turn sequentially affects collective cell behavior guiding the tissueogenesis process. Once started, maturation and growth of these structures required extensive cell remodelling in the form of cell dragging and zipper fusion, which is mediated by cell adhesion on the substrate.

### 3.2.2 Effect of surface adhesivity on hMSC behaviour

In order to demonstrate that the initial adhesion stage on the substrate profoundly affects collective cell behavior guiding the tissueogenesis process, we investigated the effect of adhesivity on structure formation and growth. In more details, we altered these through the chemical/geometrical modification of the nanopatterned surfaces. First, we depressed FA growth and maturation by using nanopatterns displaying narrower features (with respect to the 1.4  $\mu\text{m}$  pitch pattern), namely 350 nm wide ridges and 0.7  $\mu\text{m}$  pitch (Fig. 3).

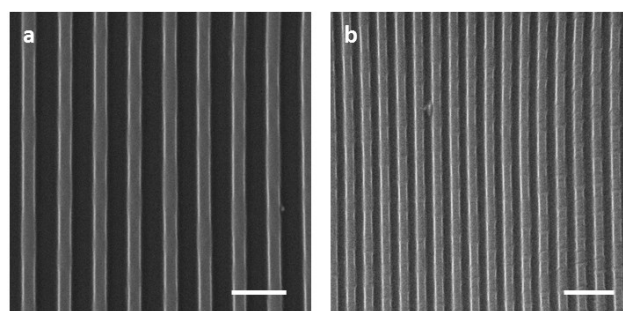


**Figure 3:** SEM images of PDMS nanopatterned substrates (a) substrate with 1.4  $\mu\text{m}$  pitch, 700 nm ridges and 700 nm grooves. (b) substrate with 0.7  $\mu\text{m}$  pitch, 350 nm ridges and 350 nm grooves. Scale bar 2  $\mu\text{m}$ .

On the 1.4  $\mu\text{m}$  pitch and 0.7  $\mu\text{m}$  pitch patterned substrates, as well as on the flat surfaces, hMSCs displayed vinculin rich FAs and a welldefined cytoskeleton (Fig 4a).

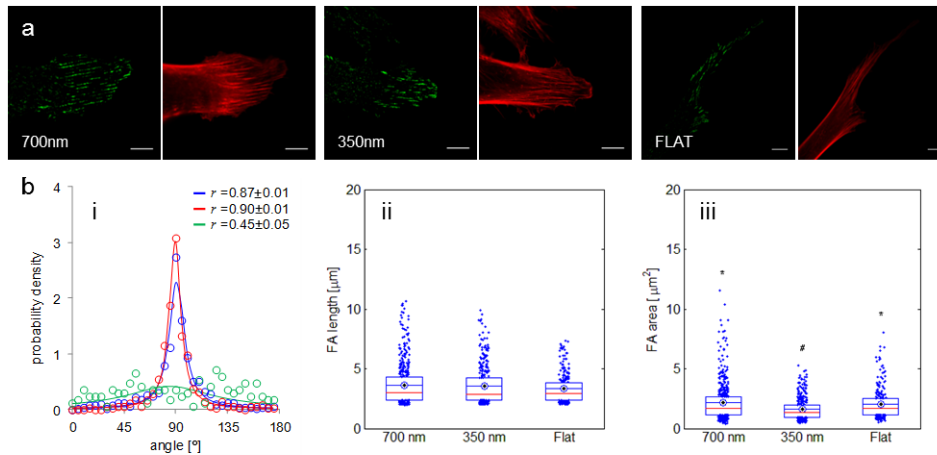


**Figure 4:** (a) Confocal images of FAs and cytoskeleton assemblies of hMSCs cultivated for 24 h on 1.4  $\mu\text{m}$  pitch patterns, 0.7  $\mu\text{m}$  pitch patterns, and flat surfaces. FAs were stained for vinculin (green) and actin bundles were stained with TRITC-phalloidin (red), scale bar 10  $\mu\text{m}$ . (b, i) Distribution of FA orientation. Open circles are the experimental data, solid lines are the wrapped Cauchy distribution fits over the experimental data (blue 1.4  $\mu\text{m}$  pitch pattern  $n = 507$ ; red 0.7  $\mu\text{m}$  pitch pattern  $n = 366$ ; green flat substrate  $n = 278$ ). Pattern direction is at  $90^\circ$ . The values of the MLE scale factor  $r$  are reported in the top right corner as mean  $\pm 95\%$  CI. (b, ii) Box plot of the focal adhesion length. (b, iii) Box plot of the focal adhesion area. Box edges define the 1st and 3rd quartile. Red line represents the median, whereas the blue target is the mean value. Columns not marked with the same symbol are significantly different ( $p < 0.05$ ).

On the 0.7  $\mu\text{m}$  pitch patterned substrates, FAs retained the same alignment (Fig. 4b i) and length (Fig. 4b ii) observed on the 1.4  $\mu\text{m}$  pitch patterned substrates, although their area was significantly smaller (Fig. 4b iii), thus indicating that the 0.7  $\mu\text{m}$  pitch patterned substrates decreased local attachment. Notably, under these conditions the hMSCs occasionally generated circular aggregates but not ordered supracellular structures (Fig. 5).

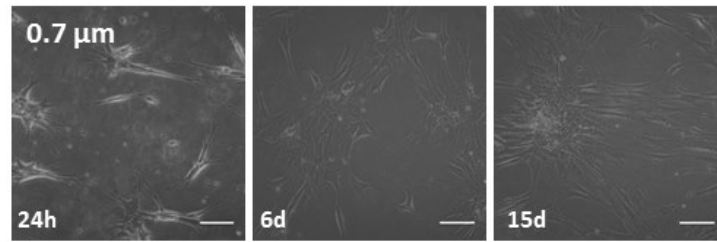


**Figure 5:** Brightfield images collected at 24 h, 6 d and 15 d of hMSCs cultivated on 0.7  $\mu\text{m}$  pitch patterns

Second, we promoted FA growth by treating the 1.4  $\mu\text{m}$  pitch patterned substrates with oxygen plasma (PT), fibronectin coating after oxygen plasma (PT+FN) and fibronectin covalent conjugation through Sulfo-SANPAH linker (SS+FN) (Fig. 6b). On the treated substrates, the FAs were highly coaligned with the pattern direction (Fig. 6b i) and were significantly longer and larger with respect to the untreated case (Fig. 6b, ii and iii). These treatments improved local attachment preserving FA orientation.

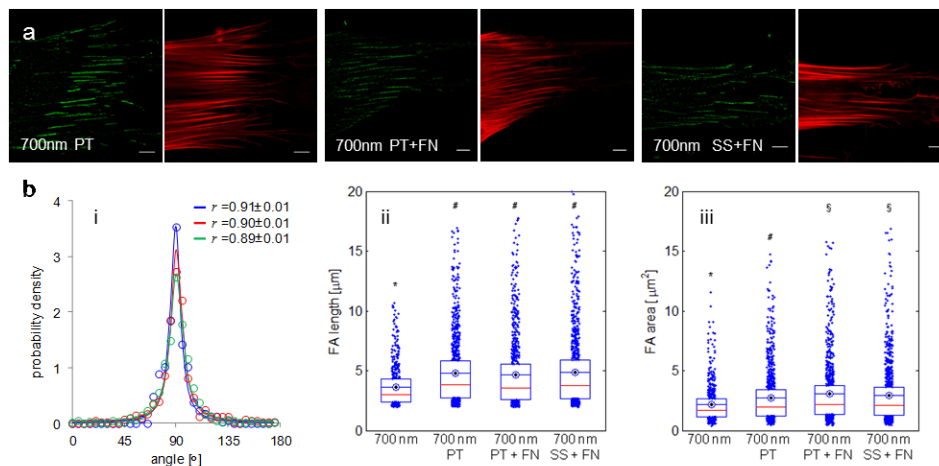


**Figure 6:** Confocal images of the FAs and cytoskeleton as in (Fig 4) for the 1.4  $\mu\text{m}$  pitch patterned substrate treated with oxygen plasma (PT), 1.4  $\mu\text{m}$  pitch patterned substrate treated with oxygen plasma and coated with fibronectin (PT+FN), and 1.4  $\mu\text{m}$  pitch patterned substrate with covalently conjugated fibronectin through Sulfo-SANPAH cross-linker (SS+FN). (d, i) Distribution of FA orientation (blue PT  $n = 955$ , red PT+FN  $n = 883$ , green SS +FN  $n = 1065$ ). (d, ii) Box plot of the focal adhesion length. (d, iii) Box plot of the focal adhesion area. Columns not marked with the same symbol are significantly different ( $p < 0.05$ )

However, when cultivated on treated surfaces the hMSCs generated a dense monolayer and were unable to form zipper-like supracellular structures (Fig. 7). After

day 10, the hMSCs spontaneously formed zones with a higher cell density nearly orthogonal to the pattern direction (Fig. 7); these, however, never developed into mature and thick structures as those observed in the untreated case. Therefore, nanopattern-induced FA confinement and polarized cell contractility appeared to be necessary for the induction of ordered supracellular structures, as their formation was not observed on flat surfaces. Moreover, an adequate level of cell attachment was required to enable cell self-organization, as hMSCs forming long and extended FAs did not produce ordered supracellular structures.

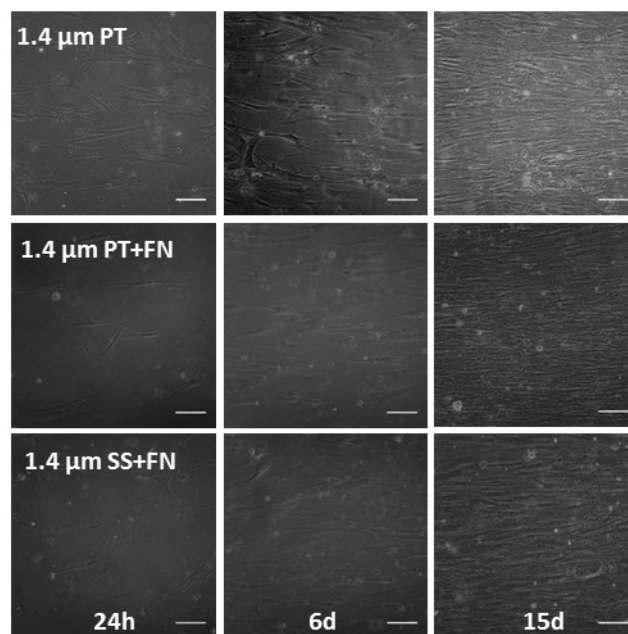


**Figure 7:** Brightfield images collected at 24 h, 6 d and 15 d of hMSCs cultivated on 1.4  $\mu\text{m}$  pitch treated patterns, namely PT, PT+FN and SS+FN.

### 3.2.3 Effect of contractility on hMSC self organization and tissue formation.

In order to modulate cell contractility, we inhibited Rho associated protein kinase (ROCK) or myosin light chain by supplementing the culture medium with either Y-27632 [13] or ML-7 [14] from day 0 onward. In presence of either inhibitor, hMSCs on the 1.4  $\mu\text{m}$  pitch pattern displayed an immature cytoskeleton with the vinculin markedly diffused in the cytoplasm (Fig. 8a). Furthermore, the formation of zippers

was not observed after 6 days of treatment (Fig. 8b). Only at longer times (10– 15 days), the cells organized aggregates similar to those generated on the untreated nanopatterns, even though they appeared thinner and lacked the characteristic cellular orientation (Fig. 8b,c).

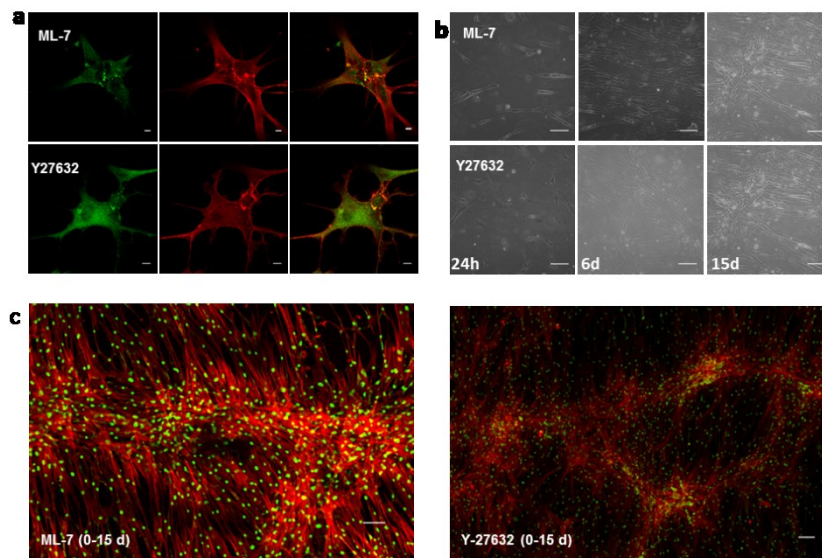


**Figure 8:** Effects of contractility inhibition on hMSC self organization. (a) hMSCs cultivated for 24 h on 1.4 μm pitch patterns in presence of ML-7 and Y-27632 inhibitor. Immunofluorescence for vinculin is in green, staining for actin is in red. Nanopattern is in the horizontal direction. Scale bar 20 μm. (b) brightfield images of hMSCs cultivated up to 15 d in presence of the actomyosin inhibitors. (c) confocal tile scan of one supracellular structure obtained after treatment with ML-7 inhibitor (left) or after treatment with Y-27632 from day 0 to day 15 of culture (right). hMSC nuclei and cytoskeleton were stained with Sytox green and TRITC-phalloidin in red, respectively. Scale bar 100 μm.

### 3.2.4 Characterization of Fibrillar Collagen by Picrosirius Red (PSR)

The self-organized structures developed on 1.4 μm pitch patterned substrates shared similarities with the tendon tissue, both in terms of macroscopic morphology and internal cellular organization. In order to gain a better insight into the spatial organization of the microconstituents, we used PSR to analyze the samples at selected time points under polarized light. Collagen production was observed already after 24

h of ascorbic acid addition (7 days post seeding), both inside and around the structures (Fig. 9a).

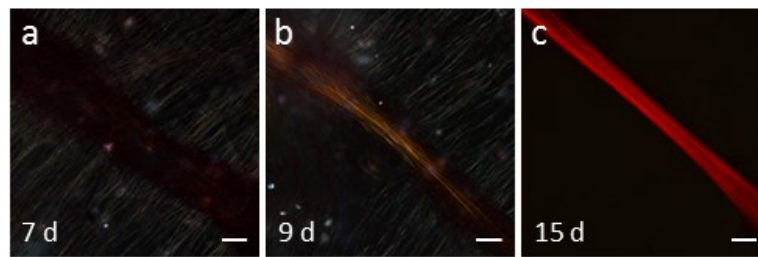


**Figure 9:** Collagen organization within the supracellular structures. Picosirus Red staining of hMSCs, seeded onto 1.4  $\mu\text{m}$  pitch patterned surfaces, visualized in polarized light (a) after 24 h culture with ascorbic acid (7 days in total) (b) after additional 48 h of culture with ascorbic acid (9 days in total) and (c) after 9 days of culture with ascorbic acid (15 days in total). Scale bar 100  $\mu\text{m}$ .

An increase in collagen production was evident after additional 48 h of culture with ascorbic acid (9 days post seeding, Fig. 9b). Later on, the staining intensity strongly increased within the structure, whereas the collagenous matrix on the nanopattern vanished. After 9 days of culture with ascorbic acid (15 days post seeding) the pattern was predominantly populated by long and intensely stained cylindrical structures (Fig. 9c). Notably, actomyosin inhibition reduced the signal detected under polarized light significantly. This occurred both when the inhibition was performed at the beginning of the cell culture or at 7 days, which we considered as the onset of tissue maturation. Even though hMSCs self-organized in structures that morphologically resembled those that formed in normal culturing conditions, matrix production and assembly was dramatically altered, and this is consistent with the role of the actomyosin machinery in the assembly and remodeling of collagen fibrils [15,16].

### 3.2.5. Transmission electron microscopy (TEM) examination

TEM examinations were performed to investigate possible interplays between hMSCs and the de novo synthesized matrix after 15 days of culture. Longitudinal sections of the central part of the shaft of the structures that formed on the 1.4  $\mu\text{m}$  pitch pattern,

showed cells closely packed in the form of parallel arrays (Fig. 10a). Nuclei also displayed an elongated morphology (Fig. 10a, b). In many cases, we observed bundles of tiny filaments, presumably actin fibers, running in parallel to the nuclear and cytoplasmic membrane (Fig. 11a). In the intercellular regions, a densely packed fibrillar matrix followed cell contours (Fig. 10a). Most fibrils were straight and directed along the 3D structure long axis. Occasionally, we also observed shorter fibrils originating in deep plasma membrane recesses or enclosed within cell compartments (Fig. 10c,d), possibly suggesting an active role of cells in remodelling the ECM at this stage of tissue maturation [16].

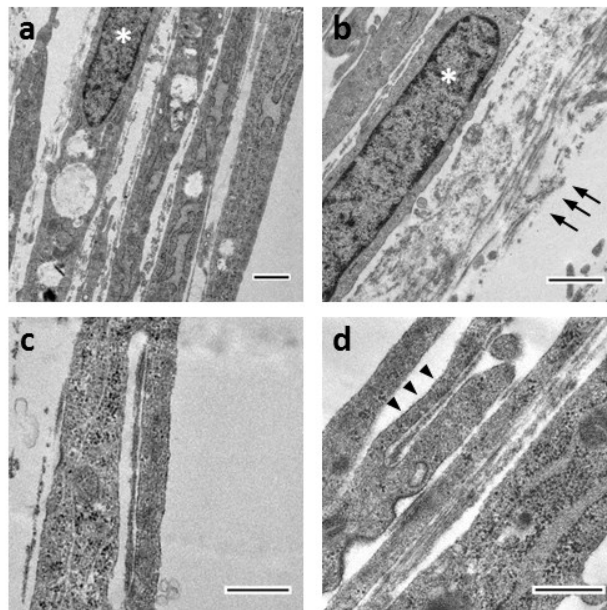


**Figure 10:** Transmission electron micrographs of the tendon-like structures. (a) Cells' bodies and nuclei (white asterisk) in the inner part of the central shaft of the structure display a high degree of coalignment, which coincides with the long axis of the structure. (b) Intercellular zones are rich in fibrillar matrix whose orientation followed cell contours (black arrows). (c) Occasionally fibrillar matrix appeared within intracellular compartments, whereas extracellular matrix was frequently observed in deep recesses of the plasma membrane (black arrowheads). Scale bar 1  $\mu\text{m}$  (a, b) and 500 nm (c, d).

However, cells constituting the outer shell had a less regular morphology, displaying several cytoplasmic vacuoles containing electron dense spots, similar to glycogen rosettes (Fig. 11b). Interestingly, we frequently observed lamellar bodies, alone or in close proximity to vacuoles (Fig. 11c, d). These structures are usually observed in those anatomical compartments that require some sort of lubrication [17]. In the case of articular joints, lamellar bodies are found in specialized fibroblast-like cells, namely type B synoviocytes, in the synovial intima that is closely connected to the tendon sheath [18]. These cells produce the synovial fluid that allows tendon gliding into the sheath cavity. Even though we do not have a thorough ultrastructural and molecular characterization of each and every cell type that constitute the in vitro produced tendon-like structure, it is tempting to speculate that a fraction of cells, in particular those located in the outer shell of the tendon-like structure, differentiate in order to synthesize the correct microenvironment to allow the tissue to become mechanically competent.

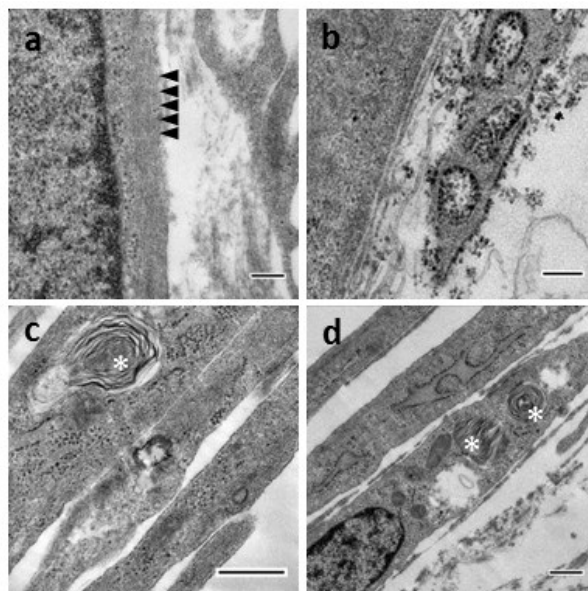


**Figure 11:** Transmission electron micrographs of tendon-like structures after 15d of culture on the 1.4  $\mu\text{m}$  pitch patterned substrate. (a) actin filaments parallel to the nucleus (black arrowheads). (b) cells on the outer shell of the structure displayed cytoplasmic vacuoles, resembling glycogen rosettes, are observed near the plasma membrane. (c) and (d) lamellar bodies (white asterisks) within cells.

Ultrastructural images of hMSC aggregates formed on flat substrates displayed different morphological features both intracellularly and in the extracellular compartments. First, hMSCs were neither densely packed nor elongated. A large number of spherical vacuoles populated the cytoplasm; most of them were predominantly located by the cell membrane. No lamellar bodies were observed among these structures. Nuclei were not elongated and displayed a convoluted membrane. Matrix was present in the extracellular space in the form of a disorganized network.

### *3.2.6. Second Harmonic Generation (SHG) Microscopy for analysis of collagen fibrillar structure*

SHG showed aligned collagen fibrils that became visible from day 10 onward. This enabled us to obtain information on the relative positioning of cells and collagen fibrils/fibers within and around the supracellular zipper-like structures that formed on the 1.4  $\mu\text{m}$  pitch pattern. Z stacked confocal images of 12 day old samples stained with TRITC-phalloidin and Sytox green revealed site-specific cellular assemblies within the structure. In particular, image analysis of the cells located on the bottom of the cylindrical structures, and thus in contact with the nanopatterned substrate, showed that their nuclei and cytoskeleton were aligned perpendicularly to the pattern direction. Collagen fibrils, observed in SHG mode, formed a dense matrix around the cells with almost the same orientation as the cell cytoskeleton (Fig. 12a). As higher focal planes were visualized, cells and nuclei strongly coaligned with the collagen matrix and the direction of orientation was nearly perpendicular to the underlying pattern (Fig. 12b). Interestingly, cells forming the outer shell were tilted of approximately  $35^\circ$  with respect to the main axis of the zipper-like structures (Fig. 12c).

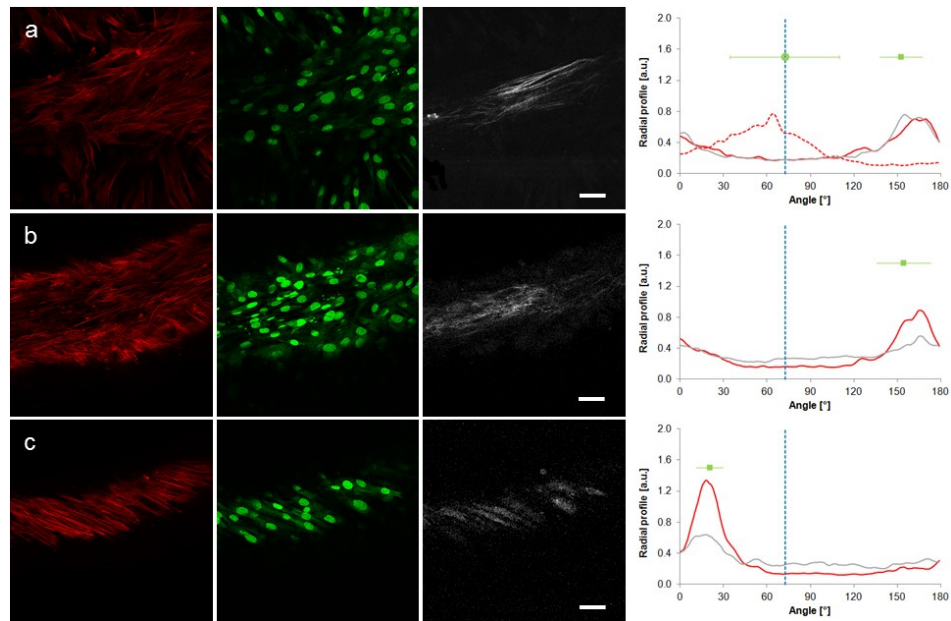


**Figure 12:** Spatial configuration of cells, nuclei, and collagen in 3D structures formed on the 1.4  $\mu\text{m}$  pitch pattern. Actin (red), nuclei (green), and collagen (gray) were visualized at different focal planes within the tendon-like structures. The analysis of the orientation in terms of the FFT power spectrum radial profile of the TRITC-phalloidin and SHG signals is reported on the right. The red dashed and solid lines represent the orientation of the cells outside and inside the structure, respectively. The gray line is the orientation of collagen fibrils visible only inside the zippers. Nuclei orientations were quantified as the orientation of the major axis of the best fitting ellipse. The open circle and solid square indicate the orientation of the nuclei outside and inside the zipper, respectively. The blue dotted line is the pattern direction. Scale bar = 20  $\mu\text{m}$ .

### 3.2.7. Molecular profile analysis by RT-PCR

To confirm the hypothesis that surface nanopatterning induce hMSC differentiation toward a tenogenic path we analyzed the expression of tenogenic early and late markers by RT-PCR along with tendon-associated adhesion and matrix molecules. The results indicated that at 10 days the expression of the early tendonspecific (SMAD8) was 6-fold significantly higher in cells grown on the 1.4  $\mu\text{m}$  pitch pattern compared to flat surface (Fig. 13a), while the late tendon-specific markers (tenomodulin and thrombospondin 4) reached the maximal up-regulation later, at 15 days (31- and 110-fold, respectively) in which case we also observed an increased expression of the tendon-related genes decorin (5-fold), collagen-I (8-fold), and collagen-III (7-fold) (Figure 5b).

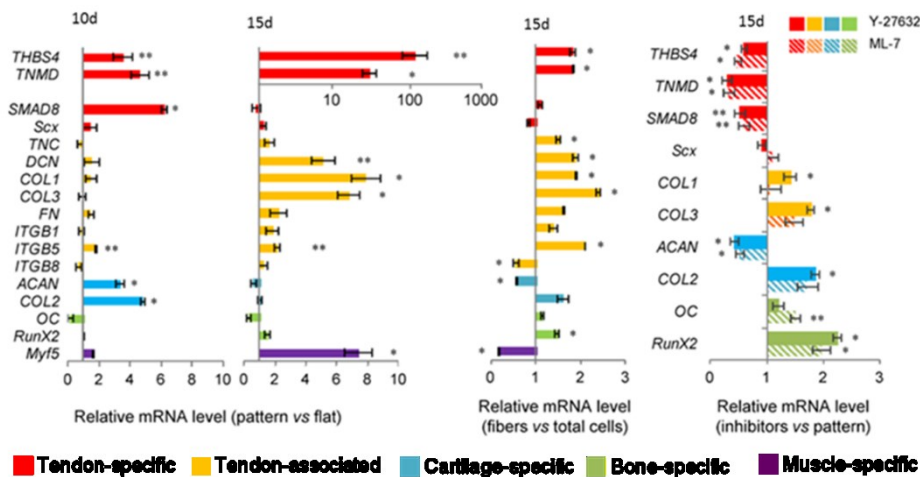


**Figure 13:** Effect of substrate matrix on tenogenic differentiation of human MSCs cultivated on 1.4  $\mu\text{m}$  pitch pattern. RT-PCR analysis of the expression at 10 days (a) and 15 days (b) of representative genes specific for tenogenic differentiation (THBS4, thrombospondin 4; TNMD, tenomodulin; SMAD8, Scx, scleraxis), tendon matrix genes (TNC, tenascin C; DCN, decorin; COL1, collagen 1; COL3, collagen 3), tendon-associated adhesion molecules (FN, fibronectin; ITGB1, integrin  $\beta$ 1; ITGB5, integrin  $\beta$ 5; ITGB8 integrin  $\beta$ 8) and chondrogenic (COL2, collagen 2; ACAN, aggrecan), osteogenic (RunX2; OC, osteocalcin F) and myogenic (Myf5, Myogenic Factor 5) differentiation markers. Relative gene expression was quantified using the  $2^{-\Delta\Delta\text{CT}}$  method by normalizing the target gene expression to GAPDH and reported in histograms as relative fold change with respect to the flat substrate. Data are shown as mean  $\pm$  SEM. Significant differences were assessed through two-tailed unpaired t-test (\*  $p < 0.001$ ; \*\*  $p < 0.01$ ). For the complete list of oligonucleotide primers see Supporting Information. (c) Expression of markers within isolated fiber structures compared to the whole plate cells (fiber and extra-fiber cells) at 15 days of hMSCs on pattern substrate. (d) Effect of 15-day treatment with either ML-7 or Y-27632 on the hMSC differentiation onto 1.4  $\mu\text{m}$  pitch pattern.

Other non tendon-associated genes were significantly up-regulated at 10 days (aggrecan 5-fold and collagen II 3.5-fold) and at 15 days (myogenic factor 5, 7-fold). This is consistent with the hMSCs differentiation potential toward mesodermal-derived fates. More interestingly, when analyzing the expression of genes involved in tendon development only in the cells making up the structures, we found that the expression of tendon-specific and –associated genes was about 2-fold higher in isolated fibers compared with the total cell population adhering to the pattern surface; we also noticed a decrease of nontendon-related genes aggrecan and

myogenic factor 5 (Fig. 13c). Even though a few nontendonrelated markers were still expressed in the structures, their overall expression levels with the exception of myogenic factor 5 were still very low (Fig. 13b). The evidence of the overexpression of the tendon-specific and -associated genes suggests therefore that the tendon-like structures generated a microenvironment supportive of the predominant tenogenic differentiation with the up-regulation of late tendon markers. Cells on the nanopattern that do not constitute the tendon-like structures are likely to differentiate toward other mesodermal lineages. Taken together, the molecular analysis supports the hypothesis of tenogenic differentiation mediated by the nanopattern, which defines the initial condition for adhesivity and therefore controls contractility. As expected, the inhibition of actomyosin contractility with ML-7 and Y-27632 induces a dramatic down-regulation of specific tendon markers (Fig. 13d).

### **3.3 Conclusions**

Our data confirm that the initial adhesive conditions provided by the nanopattern modulate the direction and magnitude of cell generated forces, eventually guiding cell selforganization and the development of highly ordered supracellular structures. Remarkably, the 1.4  $\mu\text{m}$  pitch, but not the 0.7  $\mu\text{m}$  pitch-patterned substrate, along with the adhesivity of the hydrophobic PDMS guarantees such a stringent balance. In particular, the nanopattern should initially confine and orient FAs in order to polarize the direction of cell contractile forces. However, the FA area should be sufficiently large to enable the adhesion of the cells, while allowing collective cell migration during the phases of zipper formation and structure organization. In this work, we demonstrated that surface nanopatterning is effective in directing cell self-organization, which culminates in the in vitro generation of centimeter-long and viable tendonlike tissues without the employment of growth factors or exogenous scaffold matrices. While the effect of nanopatternig has been widely investigated in

the context of cell differentiation, it has been rarely exploited to regulate cell self-organization thus obtaining tissues with predetermined architecture and functions. For example, Guillemette et al. [19] cultivated corneal fibroblasts on microtextured substrates and produced corneal equivalents displaying a lamellar microarchitecture similar to that found in native tissues and superior optical properties compared to corneal tissue grown on flat substrates. Kim et al. [20] successfully reproduced in vitro functional myocardial tissues by cultivating rat ventricular myocytes on nanotextured polyethylene glycol based materials. Strikingly, cells responded with great sensitivity to the nanometric features of the pattern by adapting their morphological, molecular, and electrophysiological characteristics. This emphasized the powerful role that nanoscale signals may have in modulating various aspects of the tissue behavior. More recently, Xing et al. [21] used synthetic nanogratings to produce aligned nanofibrous tissues that showed excellent properties in supporting hMSC growth and in mitigating inflammation response when used as a supporting scaffold. Therefore, nanopatterning can in principle dictate the microarchitecture of growing tissues and eventually their functions. However, information on the dynamics of cell self-organization and how this is regulated by the nanopatterned signals is still missing.

We reported that the guiding power of surface nanopatterning goes well beyond tissue architecture. In fact, the nanopattern coordinates cell self-organization and defines the shape of the supracellular structures, whereas an intermediate level of adhesivity enables tissue remodelling. In fact, when failing to provide them with the adequate initial cues, hMSCs do not form ordered tendon-like tissues. For instance, increasing cell–substrate adhesivity with chemical treatments favors the formation of cell monolayers. Conversely, depressing adhesivity with narrower pattern features (0.7  $\mu\text{m}$  pitch) promotes cell clustering in the form of spheroids.

Other strategies, having the common purpose of modulating adhesivity, provided analogous results. For instance, stiffer 1.4  $\mu\text{m}$  pitch patterned PDMS or hard 1.4  $\mu\text{m}$  pitch patterned polycarbonate substrates lead to monolayer formation, whereas softer 1.4  $\mu\text{m}$  pitch patterned PDMS substrates produced spherical clusters. Likewise, the inhibition of cell contractility alters the morphology of supracellular structures and tissueogenesis and, additionally, reduces the expression of tendon-specific genes. Interestingly, if inhibition starts at a point halfway the tenogenesis process, the gross structural morphology is retained; however, the inner matrix is less ordered with respect to the untreated case and the expression of tendon specific and associated markers is altered. Nanopatterning acts locally on FAs and cytoskeleton assembly. This induces cells to form densely packed structures in which cells are elongated along the structure axis, which suggests that tension arising from cell contractility is uniaxial. Conversely, on flat substrates, cells organize in the form of spheroids in which the tension that builds up is isotropic causing a different structural evolution and cellular differentiation. Besides the direction of contractile forces, tension magnitude is also important for the tenogenesis process, because alteration of cell contractility with inhibitors affects the morphology of supracellular structures as well as the internal collagen organization. Tension establishing in compacting gels also proved to have major role into the differentiation of MSCs toward tenogenesis. Kuo and Tuan highlighted the role of Scleraxis in hMSCs tenogenesis in 3D collagen gel under tension [22]. In particular, Scleraxis was upregulated when cells were cultivated in the 3D gel and tension was sufficient to induce tenogenesis, but dynamic loading was necessary to sustain the tenogenic differentiation process of the hMSCs. Other tendon associated genes as Collagen 1 and 3 increased their expression level with culturing time even in static condition, which is in agreement with our data and support the hypothesis that cell generated contractile forces are necessary for both matrix gene expression and matrix assembly in the extracellular space. More recently, Kapacee et

al. [23] reported a different trend for the Scleraxis expression of hMSCs encapsulated in a fibrin gel under tension. No significant differences between 2D or 3D culture were observed in terms of Scleraxis expression. Therefore, other than dimensionality the proteinaceous environment in which the cells reside may exert a role in Scleraxis expression. In our experiments, even though tendon-like structures on the nanopattern or cell aggregates on flat surfaces are three-dimensional, they cannot be directly compared with conventional cell culture models in 3D exogenous matrices. However, even if we did not observe a significant upregulation of Scleraxis between the 1.4  $\mu\text{m}$  pitch patterned and flat substrates, we believe that the levels of expression are sufficient to direct hMSCs toward a tenogenic differentiation pathway. In fact, Scleraxis is known to anticipate and regulate Tenomodulin expression [24]. Interestingly, we found that Scleraxis expression was increased after day 7 both on the 1.4  $\mu\text{m}$  pitch pattern and flat substrates compared to undifferentiated hMSCs, by a factor 7 and 6, respectively, while the late tendon markers tenomodulin and thrombospondin 4 remained almost undetectable. Afterward, at day 10 the expression of Scleraxis declined and the negative trend held at day 15 when the expression was 1.8 and 1.6 fold on the nanopattern and flat surfaces, respectively, greater than undifferentiated cells. Even though we did not find any significant difference between expression levels of cells on the nanopattern and flat surfaces at each time point, the average values of Scleraxis expression were consistently higher for cells cultivated on the nanopattern. Conversely, tenomodulin and thrombospondin 4 were largely up-regulated in the presence of the 1.4  $\mu\text{m}$  pitch pattern at 15 days. Finally, although both substrates support the differentiation of hMSCs toward mesodermal-derived fates, allowing the expression of early markers as Scleraxis, nevertheless only the nanopatterned substrate is able to drive the maturation of a predominant tenogenic phenotype, leading to the formation of tendon-like structures and to the up-regulation of late tendon markers (tenomodulin

and thrombospondin 4). The observation that some of the nontendon-related markers were still expressed in the tendon-like structures demands that aspects of the chemical/physical properties of the nanopatterned material need to be finely tuned in order to further enhance hMSC tenogenic differentiation over other lineages. Although we are aware that the underpinning biological mechanism is currently missing, we provided undeniable evidence of a material mediated tenogenesis, able to recapitulate in vitro crucial molecular and morphological events occurring during tendon development. In particular, by providing the initial conditions for FA assembly, hMSCs selforganize and produce tendon-like tissues in a deterministic manner. Our results open up new routes to the generation of functional tissues in vitro; in principle, by combining different arrays of patterns that control FA length and orientation and therefore cytoskeleton assembly, it would be possible to govern adhesive and contractile processes, thus guiding the spontaneous self organization of stem cells and ultimately tissuegenesis.

### 3.4 References

1. Lancaster, M. A.; Renner, M.; Martin, C. A.; Wenzel, D.; Bicknell, L. S.; Hurles, M. E.; Homfray, T.; Penninger, J. M.; Jackson, A. P.; Knoblich, J. A. *Nature* 2013, 501, 373–390.
2. Spence, J. R.; Mayhew, C. N.; Rankin, S. A.; Kuhar, M. F.; Vallance, J. E.; Tolle, K.; Hoskins, E. E.; Kalinichenko, V. V.; Wells, S. I.; Zorn, A. M.; Shroyer, N. F.; Wells, J. M. *Nature* 2011, 470, 105–109.
3. Eiraku, M.; Takata, N.; Ishibashi, H.; Kawada, M.; Sakakura, E.; Okuda, S.; Sekiguchi, K.; Adachi, T.; Sasai, Y. *Nature* 2011, 472, 51–56.
4. Lancaster, M. A.; Knoblich, J. A. *Science* 2014, 345, 1247125.
5. Ader, M.; Tanaka, E. M. *Curr. Opin. Cell Biol.* 2014, 31, 23–28.
6. Mammoto, T.; Ingber, D. E. *Development* 2010, 137, 1407–1420.
7. Schwarz, U. S.; Gardel, M. L. *J. Cell. Sci.* 2012, 125, 3051–3060.
8. Eyckmans, J.; Boudou, T.; Yu, X.; Chen, C. S. *Dev. Cell.* 2011, 21, 35–47.
9. Teo, B. K. K.; Wong, S. T.; Lim, C. K.; Kung, T. Y. S.; Yap, C. H.; Ramagopal, Y.; Romer, L. H.; Yim, E. K. F. *ACS Nano* 2013, 7, 4785–4798.
10. Engler, A. J.; Sen, S.; Sweeney, H. L.; Discher, D. E. *Cell* 2006, 126, 677–689.
11. Natale, C. F.; Ventre, M.; Netti, P. A. *Biomaterials* 2014, 35, 2745–2751.
12. Zeitouni, S.; Krause, U.; Clough, B. H.; Halderman, H.; Falster, A.; Blalock, D. T.; Chaput, C. D.; Sampson, H. W.; Gregory, C. A. *Sci. Transl. Med.* 2012, 4, 132–155.
13. Narumiya, S.; Ishizaki, T.; Uehata, M. *Methods Enzymol.* 2000, 325, 273–284.
14. Hale, C. M.; Sun, S. X.; Wirtz, D. *PLoS One* 2009, 4, e7054.
15. Canty, E. G.; Starborg, T.; Lu, Y.; Humphries, S. M.; Holmes, D. F.; Meadows, R. S.; Huffman, A.; O’Toole, E. T.; Kadler, K. E. *J. Biol. Chem.* 2006, 281, 38592–38598.
16. Kalson, N. S.; Starborg, T.; Lu, Y.; Mironov, A.; Humphries, S. M.; Holmes, D. F.; Kadler, K. E. *Proc. Natl. Acad. Sci. U.S.A.* 2013, 110, E4743–E4752.

17. Schmitz, G.; Müller, G. J. *Lipid Res.* 1991, 32, 1539–1570.
18. Kohama, M.; Nio, J.; Hashimoto, Y.; Iwanaga, T. *Jpn. J. Vet. Res.* 2002, 50, 125–139.
19. Guillemette, M. D.; Cui, B.; Roy, E.; Gauvin, R.; Giasson, C. J.; Esch, M. B.; Carrier, P.; Deschambeault, A.; Dumoulin, M.; Toner, M.; Germain, L.; Veres, T.; Auger, F. A. *Integr. Biol.* 2009, 1, 196–204.
20. Kim, D. H.; Lipke, E. A.; Kim, P.; Cheong, R.; Thompson, S.; Delannoy, M.; Suh, K. Y.; Tung, L.; Levchenko, A. *Proc. Natl. Acad. Sci. U.S.A.* 2010, 107, 565–570.
21. Xing, Q.; Vogt, C.; Leong, K. W.; Zhao, F. *Adv. Funct. Mater.* 2014, 24, 3027–3035.
22. Kuo, C. K.; Tuan, R. S. *Tissue Eng., Part A* 2008, 14, 1615–1627.
23. Kapacee, Z.; Yeung, C. Y.; Lu, Y.; Crabtree, D.; Holmes, D. F.; Kadler, K. E. *Matrix Biol.* 2010, 29, 668–677.
24. Shukunami, C.; Takimoto, A.; Oro, M.; Hiraki, Y. *Dev. Biol.* 2006, 298, 234–247.

## 4. Materials and methods

### 4.1 Preparation of nanopatterned substrates

Patterned substrates were obtained by replica molding of polydimethylsiloxane, PDMS (Sylgard 184, Dow Corning) on a polycarbonate master. The patterns consisted of an area of 4 cm<sup>2</sup> containing parallel and straight channels having a ridge to groove width ratio of 1:1, pattern pitch of 1.4 μm and groove depth of 250 nm. PDMS was prepared by mixing elastomer base and curing agent at a 10:1 weight ratio. Softer or stiffer substrates were prepared by mixing base to curing agent at 10:0.5 or 10:2 weight ratio respectively. A second polycarbonate master was used to fabricate patterns with narrower features, namely 0.7 μm pitch (1:1 groove to ridge width) and 100 nm depth. For all experimental conditions PDMS solution was degassed, poured onto the polycarbonate master and then cured at 37 °C for 24 h. Control (flat) PDMS substrates were produced by pouring the base and curing mix on a 35 mm polystyrene Petri dish (Corning) and curing at 37 °C for 24 h. Substrates were sterilized in autoclave and then incubated with a serum supplemented culture medium overnight prior to the cell culturing experiment. Polycarbonate masters (1.4 μm pitch, 1:1 groove to ridge width and 250 nm depth) were also used as cell culture substrates, in which case the masters were preincubated in serum-supplemented medium as previously described.

### 4.2 Functionalization of patterned surfaces.

Substrate adhesivity was modulated by oxygen plasma treatment, fibronectin coating or fibronectin covalent conjugation. The first case consisted in exposing the 0.7 and 1.4 μm pitch patterned PDMS substrates to the oxygen plasma treatment for 1 min and then incubating them with the serum-supplemented culture medium overnight prior to cell seeding (samples referred to as PT). In the second case, 1.4 μm pitch patterned PDMS substrates were treated with oxygen plasma (1 min) and then the

samples were incubated with a 10 µg/ml fibronectin solution (Sigma) in PBS overnight at 4 °C (samples referred to as PT+FN). In the last case fibronectin was covalently conjugated to the nanopatterned substrates with NSulfosuccinimidyl- 6-(4'-azido-2'-nitrophenylamino) hexanoate crosslinker (Sulfo – SANPAH, Thermo Scientific). 1.4 µm pitch patterned PDMS substrates were exposed to the oxygen plasma treatment for 1 min and then were incubated with the solution of Sulfo – SANPAH (0.5 mg/ml in 350 mM HEPES buffer, pH 8.5). The surfaces were illuminated with UV light, 365 nm, for 10 min. The excess of Sulfo – SANPAH was removed and the surfaces were exposed to additional 10 min of UV treatment to complete the coupling reaction. The substrates, washed twice in PBS, were then incubated with the fibronectin solution (10 µg/ml in PBS) and stored overnight at 4 °C (samples referred to as SS+FN). Plasma treatments were performed with a Plasma Femto (Diener) equipped with 13.56 MHz 50W generator for the plasma excitation.

### *4.3 Cell culture*

Human Mesenchymal Stem Cells (hMSCs) were purchased from Lonza. hMSCs were cultured in α-MEM (Modified Eagle's Medium, Bio Whittaker) supplemented with 10% fetal bovine serum (FBS, Euroclone), 100 mg/ml L-glutamine, 100 U/ml penicillin/streptomycin (Sigma). hMSC were used at passage 3.

The MG63 osteosarcoma cell line and NIH3T3 mouse fibroblast (ATCC) were cultured in Dulbecco's modified Eagle medium (DMEM) supplemented with 10% fetal bovine serum (FBS, Biowittaker), 100 mg/ml L-glutamine, 100 U/ml penicillin/streptomycin (Sigma).

MC3T3-E1 preosteoblasts (ATCC) were cultured in αMEM (Gibco) with deoxyribonucleosides, ribonucleosides and 2 mM L-glutamine, supplemented with 10% foetal bovine serum (Biowittaker) and 100 U/ml penicillin/streptomycin (Sigma). Human dermal fibroblasts (neonatal HDF 106-05n ECACC) were sub-cultured in EMEM

culture medium (Eagle's BSS Minimum Essential Medium) containing 20% fetal bovine serum (Biowittaker), 100 mg/ml L-glutamine, 100 U/ml penicillin/streptomycin, and 0.1 mM non essential amino acids (Sigma). All cell lines were kept in a humidified atmosphere at 37 °C and 5% of CO<sub>2</sub>. The medium was replaced every 3 days. After 3 days of culture, cells were detached with trypsin/EDTA (0.25% w/v trypsin /0.02 mM EDTA) (Sigma) and seeded on nanopatterned or flat surfaces. Cells were seeded onto the surfaces at the density of 10<sup>3</sup> cells/cm<sup>2</sup>. After 7 days of culture, to promote the development and stability of extracellular matrix, the basal medium was enriched with an ascorbic acid solution (50 µg/ml) (Sigma).

#### *4.4 Drug treatment*

Y-27632 (Rho-associated protein kinase inhibitor, Sigma) and ML-7 (myosin light chain kinase inhibitor, Sigma) were used to inhibit cell contractility. Cell culture media were supplemented with either a solution of Y-27632, (10 µM in DMSO) or ML-7 (20 µM in DMSO). The incorporation of the inhibitor solution to the culture was performed every 2 days to expose cells to active inhibitors. Also for Y-27632 or ML-7 treated hMSCs, ascorbic acid was added at the beginning of day 7 at the same concentration. In order to assess a possible effect of drugs treatment on cell proliferation, hMSCs treated either with Y-27632 or with ML-7 were trypsinized (0.25% w/v for 5 min) and counted at 24 h, 3 d, 7 d and 15 d post plating using a Neubauer chamber. hMSCs cultivated in normal conditions were used as control. At least three measurements per each sample and per each time point were performed. All the experiments were performed in triplicate. Significant differences were assessed with ANOVA test followed by a Tukey's post-hoc test performed in Matlab (The MatWorks). Data were considered significantly different for  $p < 0.001$ .

#### *4.5 Time lapse video microscopy*

In order to observe and characterize, both single and collective cell migratory behavior, the migration of hMSC was monitored by time lapse experiments performed using an inverted phase contrast microscope (Olympus) with either 4X or 10X magnification lens equipped with an incubation chamber (37°C, 5% CO<sub>2</sub>), a x-y computer- controlled stage (PROSCAN; Prior, USA) and a charge coupled device (CCD) coolsnap camera (RS Photometrix, USA). Camera and computerized stage were synchronized by a specific code to follow several cells migration during the same experiments.

Images, captured every 20 min over 24 h time interval, were analyzed by using the image analysis software Metamorph 5.0.

#### *4.6 Confocal and multiphoton microscopy*

Actin fibers, fibronectin fibers, focal adhesions and nuclei were visualized with confocal microscopy. Briefly, cells cultured on nanopatterned or flat surfaces were fixed in paraformaldehyde 4% (w/v) (Sigma) for 20 min at room temperature (RT), then samples were washed with PBS and incubated with 0.1% PBS-Tryton X-100 (Sigma) solution. After 10 min at RT, the substrates were rinsed twice with PBS and non specific antigenic sites were saturated with PBS-BSA 1% (Sigma) for 30 min. Focal adhesions were recognized by marking vinculin through immunofluorescence. Samples were incubated with antivinculin monoclonal antibody (dilution 1:200, Millipore) for 2 h at RT. After incubation, surfaces were washed three times with PBS and incubated with Alexa Fluor 488 conjugated goat anti-mouse antibody (dilution 1:1000, Molecular Probes) for 30 min at RT. Actin filaments were stained with TRITC-conjugated phalloidin (dilution 1:200; Sigma) for 30 min at RT.

The fibronectin fibers were recognized by marking fibronectin through immunofluorescence. Samples were incubated with antifibronectin monoclonal

antibody (dilution 1:100, SIGMA) for 2 h at RT. After incubation, surfaces were washed three times with PBS and incubated with ATTO 647 conjugated goat anti-mouse antibody (dilution 1:300, SIGMA) for 30 min at RT. Cell nuclei were stained by incubating samples with Sytox green (1:1000 in PBS, Invitrogen) for 15 min at 37 °C. Digital images of actin filaments, fibronectin fibers and focal adhesion were collected with a LSM Confocor 710 confocal microscope (Zeiss). TRITC- phalloidin conjugated actin fibres were excited with a 543 nm He-Ne laser and emitted radiation was collected in the 560-600 nm interval. Alexafluor conjugated vinculin was excited with a 488 Ar laser and the emission was collected in the 500- 530 nm interval. ATTO conjugated fibronectin was excited with a 633 laser and the emission was collected in the 630-700 nm interval.

A 40x water immersion objective lens was used to acquire the images with zoom spanning in the 1 – 1.5 range. Resolution was automatically adjusted using the command “highest” of the confocal microscope software to 0.086 µm/pixel. Digital images of actin fibres, nuclei and collagen were acquired with a Leica TCS SP 5 multiphoton confocal microscope (Leica Microsystems). TRITC –phalloidin conjugated actin was visualized as described above. Sytox green stained nuclei were excited with 488 nm Ar laser and the emission was collected in the 500-530 nm interval.

#### *4.7 Image analysis*

Digital images of FAs were first processed using blur command by following a modified procedure of the one proposed by Maruoka et al.<sup>1</sup> Briefly, a copy of the digital image of vinculin stained cells was filtered with a 15 pixel Gaussian blur filter in Fiji.<sup>2</sup> Blurred image was then subtracted from the original image using the image calculator command. The image was further processed with an Otsu threshold command to

obtain a binarized image. Pixel noise was erased using the erode command (iter=2; count=4) and then particles analysis was performed in order to extract the morphometric descriptors. Only focal adhesions whose Feret length was above 2  $\mu\text{m}$  were taken into account for the statistical analysis. Statistical significance was computed using the Kruskal-Wallis test, followed by the Tukey's post-hoc test in Matlab (The MathWorks). The distribution of focal adhesion orientation angle was fitted with a wrapped Cauchy distribution. Data fitting was performed with the Maximum Likelihood Estimates in Matlab.

#### *4.8 Characterization organization of the collagen fibers*

Collagen fibers assembly and arrangement were observed by means of Picrosirius Red stain and polarized light. Briefly, cells cultivated on the 1.4  $\mu\text{m}$  pitch pattern or flat substrates were fixed in 10% formalin overnight at 4 °C, washed with PBS. Picrosirius Red solution was prepared by mixing Sirius Red (Direct Red 80, Sigma) and saturated aqueous solution of picric acid 0.15 (w/v). The samples were incubated for 60 min at RT. After incubation the substrates were rinsed with aqueous acetic acid solution (0.5% in H<sub>2</sub>O). Dehydration was performed through a series of ethanolic baths (75%, 85%, 95%, 100%). Samples were dried under the extractor hood and Picrosirius Red stained sections were mounted on glass slides with Biomount (Bio Optical). Slides were observed with a Olympus BX53 upright microscope under polarized light equipped with either a 10x or a 20x objective lens.

#### *4.9 Second harmonic generation*

Another method to assess the arrangement of the collagen fibers within cell structures is the Second Harmonic Generation (SHG). SHG has been established as a

viable microscope imaging contrast mechanism for visualization of cell and tissue structure and function. A second-harmonic microscope obtains contrasts from variations in a specimen's ability to generate second-harmonic light from the incident light while a conventional optical microscope obtains its contrast by detecting variations in optical density, path length, or refractive index of the specimen. SHG requires intense laser light passing through a material with a noncentrosymmetric molecular structure. Second-harmonic light emerging from an SHG material is exactly half the wavelength (frequency doubled) of the light entering the material.

Though SHG requires a material to have specific molecular orientation in order for the incident light to be frequency doubled, some biological materials can be highly polarizable, and assemble into fairly ordered, large noncentrosymmetric structures. Biological materials such as collagen, microtubules, and muscle myosin can produce SHG signals. The SHG pattern is mainly determined by the phase matching condition. A common setup for an SHG imaging system will have a laser scanning microscope with a titanium sapphire mode-locked laser as the excitation source. The SHG signal is propagated in the forward direction. However, some experiments have shown that objects on the order of about a tenth of the wavelength of the SHG produced signal will produce nearly equal forward and backward signals. Collagen fibrils were visualized through second harmonic generation microscopy, i.e. samples were excited with a femtosecond laser (Coherent) at 840 nm and the emission was collected in the 415-425 nm interval.

#### *4.10 Transmission electron microscopy (TEM)*

Transmission electron microscopy was performed on tendon-like tissues or cell aggregates formed at 15 d post seeding on the 1.4  $\mu\text{m}$  pitch pattern or flat substrates respectively. Samples were fixed in 2.5% (v/v) glutaraldehyde (SIC) for 2 h at RT in 0.1 M sodium cacodylate buffer (pH 7.3, SIC), washed three times for 10 min in 0.1 M

sodium cacodylate buffer (pH 7.3), then post-fixed in 1% osmium tetroxide (Sigma) in sodium cacodylate buffer (0.1 M, pH 7.3). Samples were washed three times and then they were dehydrated in ascending series of ethanol and embedded in Spurr's resin (SIC). Thin sections (70 nm) were obtained with a EM UC6 ultramicrotome (Leica) equipped with a diamond knife (Diatome). Sections were collected on uncoated 200 mesh thin bar copper grids and stained for 10 min with 2% uranyl acetate and for 8 min in Reynold's lead citrate (Electron Microscopy Science). Sections were observed at a Tecnai G2 transmission electron microscope (FEI) at 80 KV and images were acquired with an Eagle 2K high sensitivity camera (FEI).

#### *4.11 Scanning electron microscopy (SEM)*

SEM analysis was performed on hMSC cell sheets formed at 20 d post seeding on HARD, MEDIUM and SOFT PT 0.7  $\mu\text{m}$  pitch PDMS. As for the TEM preparative, samples were fixed in 2.5% (v/v) gluteraldehyde (SIC) for 2 h at RT in 0.1 M sodium cacodylate buffer (pH 7.3, SIC), washed three times for 10 min in 0.1 M sodium cacodylate buffer (pH 7.3), then post-fixed in 1% osmium tetroxide (Sigma) in sodium cacodylate buffer (0.1 M, pH 7.3). Samples were washed three times and then they were dehydrated in ascending series of ethanol (40% to 100%). The final changes of ethanol must be conducted using anhydrous ethanol. Typically three changes of anhydrous ethanol are used. In order to prevent damage to the specimens during air drying, the critical point drying technique is frequently employed. A critical point drier (CPD, Leica) was used to replace all of the ethanol with liquid carbon dioxide under pressure. The pressure and temperature were raised in the CPD until the specimen was above the triple point at which time it is safe to decrease the temperature and release the pressure. The volume of liquid carbon dioxide was replaced several times until ethanol was no longer present in the purge line. One or two additional changes of

liquid carbon dioxide were typically used in order to assure that no ethanol is present during the drying stage. Specimens were mounted on stubs and gold sputtered.

#### 4.12 Nano-indentation test

Nano-indentation test were performed by means of Piuma Nano-Indenter (Optics11). Briefly, the tip penetrates within the samples surface up to a predefined value. The Young's modulus of the material is derived from the load-displacement curve by applying the Oliver and Pharr method for spherical indenters (Oliver and Pharr 2004). The method evaluates the Young's modulus from the slope of the unloading part of the load-displacement curve by means of the equation:

$$E^* = \frac{S}{2} \frac{1}{\sqrt{R_{tip}(h - h_{fin})}}$$

in which  $E^*$  is the effective Young's modulus,  $R_{tip}$  is the spherical tip radius,  $S$  the slope at maximum indentation and  $h$  and  $h_{fin}$  the maximum indentation depth and final contact depth after unloading, respectively. The cantilever is positioned at the end of an optical fiber, such that the cantilever covers the end of the fiber. A spherical tip of 78  $\mu\text{m}$  is attached to the end of the cantilever, and is then used to indent the sample by applying a known displacement to the whole probe. The optical fiber is used to measure the cantilever deflection during the indentation that, given the cantilevers stiffness, correlates to the applied load and, combined with the probe displacement, also gives the indentation depth.

#### 4.13 Real Time-PCR

Quantitative PCR was performed on hMSCs seeded onto the 0.7  $\mu\text{m}$  pitch patterned surfaces, to analyze the expression of stemness, pluripotency, matrix and differentiation markers in the formed cell sheet and on hMSCs seeded onto the 1.4

µm pitch patterned surfaces in order to establish the expression of tendon-specific and tendon-associated genes involved in tenocyte development. In this latter case, mRNA levels of specific markers for cartilage, bone and muscle differentiation were also evaluated. Total RNA was extracted with the Perfect Pure RNA Cultured Cell Kit (5 Prime Inc), following the manufacturer's instructions and cDNA was synthesized by using the EuroScript M-MLV Reverse Transcriptase (Euroclone). The expression level of representative tissue-specific genes was evaluated by RT-PCR using the Fluocycle II SYBR Green Master mix (Euroclone). Specific primers were designed by using the NCBI Primer-BLAST web resource and purchased from Sigma-Aldrich. The relative fold change in gene expression was quantified using the  $2^{-\Delta\Delta CT}$  method by normalizing the target gene expression to GAPDH and relative to the expression on the experimental control sample, as indicated in Figure 5. Data are the means  $\pm$  SEM of triplicate samples of at least two independent experiments. For statistical significance, p-values were calculated by using a two-tailed unpaired t-test (independent samples, unequal variance). The complete list of oligonucleotide primers was reported below.

Marker housekeeping

**GAPDH:** forward primer 5'-GGAGTCAACGGATTTGGTCGT-3'

reverse primer 5'- GCTTCCCGTTCTCAGCCTTGA -3'

Markers of Tenogenic differentiation:

Early:

**Scleraxis:** forward primer 5'-CCTGAACATCTGGGAAATTTAATTTTAC-3'

reverse primer 5'-CGCCAAGGCACCTCCTT-3'

**SMAD8:** forward primer 5'-TGCCACAGCTGATAGACACG-3'

reverse primer 5'-AGGGTCGGTGAACCCATCTA-3

**Tenascin C:** forward primer 5'-TTTCTGACATAACTCCCGAGAGC-3'

reverse primer 5'-AGATATGGGCAGTTCG TTCAGC-3'

**Collagen III:** forward primer 5'-TGGAGGATGGTTGCACGAAA-3'

reverse primer 5'-ACAGCCTTGCGTGTTCGATA-3'

**Collagen I:** forward primer 5'-CAGCCGCTTCACCTACAGC-3'

reverse primer 5'-TTTTGTATTCAATCACTGTCTTGCC-3'

Late:

**Thrombospondin 4:** forward primer 5'-CGACCGAGGTTCAACGCAC-3'

reverse primer 5'-CCAGCATGTTGGCTCTTCCT-3'

**Tenomodulin:** forward primer 5'-GCCTATGACATGGAGCACACT-3'

reverse primer 5'-TCAGTGCCATTTCCGCTTCT-3'

**Decorin:** forward primer 5'-AATTGAAAATGGGGCTTTCC-3'

reverse primer 5'-GCCATTGTCAACAGCAGAGA-3'

Markers associated to Tenogenic differentiation

**Fibronectin:** forward primer 5'-ACCAACCTACGGATGACTCG-3'

reverse primer 5'-GTCATCATCTGGCCATTTT-3'

**Integrin  $\beta$ 1:** forward primer 5'-CATCTGCGAGTGTGGTGTCT-3'

reverse primer 5'-GGGGTAATTTGTCCCGACTT-3'

**Integrin  $\beta$ 5:** forward primer 5'-ACAAGGGAGTCCTCTGCTCA-3'

reverse primer 5'-GGGGCACTTCTCACACATCT-3'

**Integrin  $\beta$ 8:** forward primer 5'-ACCCCTCACTAGGCCAACTT-3'

reverse primer 5'-GCCTGTACCTGGTTTTCCA-3'

Markers of Osteogenic differentiation:

Early:

**Runx2:** forward primer 5'-CGCCTCACAACAACCACAG-3'

reverse primer 5'-GGTAGTGACCTGCGGAGATT-3'

Late:

**Osteocalcin F:** forward primer 5'-TGCAGAGTCCAGCAAAGGTG-3'

reverse primer 5'-GATGTGGTCAGCCAACTCGTC -3'

Markers of Chondrogenic differentiation:

**Aggrecan:** forward primer 5'-GAGTGGGCGGTGAGGAGGACAT-3'

reverse primer 5'-CTGCGGCGCCGTGGGGGAGA-3'

**Collagen II:** forward primer 5'-GCCACCGTGCCCAAGAAGAACT-3'

reverse primer 5'-ACAGCAGGCGCAGGAAGGTCAT-3'

Markers of Myogenic differentiation:

Early expression:

**Myf5:** forward primer 5'-GCAGGATGGACGTGATGGAT-3'

reverse primer 5'-ACTCGTCCCCAAATTCACCC-3'

**MyoD:** forward primer 5'-CCAGAGCTGAACCTTGAGGG-3'

reverse primer 5'-ACCTGCTACATTTGGGACCG-3'

Late expression:

**Myogenin:** forward primer 5'-AGATTGTCTTCCAAGCCGGG-3'

reverse primer 5'-CTGGCTCCTAGCATCAGGG-3'